Genome-wide screening reveals producer-cell modifications that improve virus-like particle production and delivery potency

Diana Ly[1], Hyewon Jang[1], Adhiraj Goel[1], Arnav Singh[1], Aditya Raguram[1,2]*

[1] Whitehead Institute for Biomedical Research, Cambridge, MA, USA

[2] Merkin Institute for Transformative Technologies in Healthcare, Broad Institute of MIT and Harvard, Cambridge, MA, USA

* Correspondence: araguram@wi.mit.edu (A.R.)

Abstract

Engineered virus-like particles (eVLPs) are promising vehicles for transient delivery of gene editing agents. While extensive particle engineering has yielded efficient eVLPs, it remains underexplored whether engineering the cells used to produce eVLPs could further improve eVLP properties. We developed a genome-wide screening approach to systematically investigate how genetic perturbations in producer cells influence eVLP production. This approach generates eVLPs loaded with guide RNAs that identify the genetic perturbation in the cell that produced a particular particle; the abundance of each guide RNA in eVLPs therefore reflects how the corresponding genetic perturbation influences eVLP production or cargo loading. We applied this approach to identify several genes that regulate eVLP cargo expression and loading into particles during the production process. Leveraging these insights, we engineered producer cells that support increased eVLP cargo packaging and a 2- to 9-fold increase in eVLP delivery potency across several cargo, particle, and target-cell types in cultured cells and in mice. Our findings suggest the potential of producer-cell engineering as a useful strategy for improving the utility of eVLPs and related delivery methods.

Introduction

Methods for safely and efficiently delivering macromolecules into cells in culture (*in vitro*) and within the body (*in vivo*) are required for many therapeutic strategies, including gene editing therapies[1-5]. Recently, virus-like particles (VLPs) have emerged as promising vehicles for therapeutic macromolecule delivery that combine key advantages of canonical viral and non-viral delivery strategies[1,6]. In typical VLPs, viral scaffold proteins are used to package and deliver cargo proteins, ribonucleoproteins (RNPs), or mRNAs instead of viral genetic material, which leads to transient cargo delivery into recipient cells[1,6]. Several VLP-based delivery methods have proven particularly effective for gene editing applications[7-23] and offer an ideal combination of efficient on-target editing, minimal off-target editing, and programmable cell-type targeting capabilities. Current state-of-the-art VLPs, including engineered VLPs (eVLPs)[7,8,22], have achieved efficient *in vitro* gene editing in primary human cells and therapeutic *in vivo* gene editing in the mouse liver and retina, highlighting the utility of eVLP delivery for research and potential therapeutic applications.

While extensive engineering of eVLP components and particle architectures has afforded efficient eVLPs[7,8,22], further improvements to eVLP properties are still required to maximize their utility. In particular, improving eVLP cargo packaging per particle or overall particle yield from the eVLP production process would enable more efficient gene editing with lower eVLP doses and simplify the production of eVLPs for large-scale studies. Standard methods for producing eVLPs involve the use of human producer cells to express eVLP components and assemble functional particles[7,8,22], suggesting that producer cells likely play an important role in the eVLP production process. Indeed, producer-cell engineering has previously been used to improve the production of lentiviral vectors and adeno-associated viral vectors[24-29]. However, previous studies have focused solely on particle engineering to improve eVLP properties, and none have explored whether producer-cell engineering could improve eVLP properties beyond what can be achieved through particle engineering alone.

In this study, we systematically investigated how genetic perturbations in producer cells influence eVLP production and applied our findings to improve eVLP production and delivery potency. Using an unbiased genome-wide screening approach in which eVLP-

packaged guide-RNA cargos directly correspond to producer-cell genetic perturbations, we identified several genes that impact eVLP production, including genes that are uniquely relevant for packaging RNP cargos into genome-free eVLPs. Guided by these observations, we engineered producer cells that support improved eVLP production and delivery potency across several cargo, particle, and target-cell types in cultured cells and in mice. Our results lay a foundation for using producer-cell engineering to improve the utility of eVLPs and related bioparticle-based delivery methods.

Results

Genome-wide screening reveals producer-cell perturbations that influence eVLP production

We began by developing an unbiased genome-wide screening approach to identify genetic perturbations in producer cells that influence eVLP production (Fig. 1a). We envisioned a general scheme in which eVLP production is initiated from a pool of genetically perturbed producer cells. Each producer cell in this pool expresses a Cas9-based genome modifying agent and a single copy of a guide RNA (sgRNA) that directs the installation of a specific genetic perturbation into that particular cell (Fig. 1a). Because eVLPs package Cas9-based cargos, the perturbation-inducing sgRNA expressed in a given producer cell is also loaded into any particles produced by that particular cell (Fig. 1a). Therefore, the abundance of a particular sgRNA in eVLPs reflects how the corresponding genetic perturbation influences eVLP production or cargo loading: sgRNAs that are more abundant identify perturbations that increase eVLP production or cargo loading, while sgRNAs that are less abundant identify perturbations that decrease eVLP production or cargo loading (Fig. 1a).

We used this general approach to perform a genome-wide knockout screen for cargo-loaded eVLP production in Gesicle 293T producer cells, a standard cell line used for eVLP production[7,8,22]. We transduced producer cells at a low multiplicity of infection (MOI) with a lentiviral sgRNA library containing 98,077 unique sgRNAs targeting 19,707 genes across the human genome[30] (Extended Data Fig. 1a). Each vector in the library also encoded constitutive expression of Cas9 nuclease. After selecting for Cas9 expression and expanding the transduced cells to generate a pool of single-knockout

89 producer cells, we initiated fourth-generation (v4) adenine base editor (ABE)-eVLP
90 production from these cells (Extended Data Fig. 1a). Importantly, to initiate eVLP
91 production, we only transfected plasmids encoding the expression of v4 ABE-eVLP
92 protein components: (1) the gag–ABE (capsid–cargo) fusion, (2) the Moloney murine
93 leukemia virus (MMLV) gag–pro–pol polyprotein, and (3) the vesicular stomatitis virus G
94 (VSV-G) envelope protein. No additional sgRNA-encoding plasmid was transfected,
95 ensuring that all eVLPs produced from a given producer cell packaged cargo containing
96 the specific knockout-inducing sgRNA that was already introduced into that producer cell
97 by lentiviral transduction (Fig. 1a and Extended Data Fig. 1a).

98 Following eVLP production, we isolated RNA from purified eVLPs and compared
99 this eVLP-packaged RNA to cellular RNA that was isolated from the single-knockout
100 producer-cell pool immediately prior to eVLP production (Fig. 1a and Extended Data Fig.
101 1a). To compare sgRNA abundances across both populations, we subjected both RNA
102 pools to template-switching reverse transcription[31], which enabled amplification and
103 sequencing of the spacer sequence at the 5' end of each sgRNA molecule (Extended
104 Data Fig. 1b). sgRNAs that are more abundant in the eVLP-packaged RNA compared to
105 the producer-cell RNA identify gene knockouts that increase eVLP production or cargo
106 loading, while sgRNAs that are less abundant identify gene knockouts that decrease
107 eVLP production or cargo loading (Fig. 1a and Extended Data Fig. 1a).

108 By aggregating the results for all sgRNAs targeting the same gene into gene-level
109 phenotypes, we determined the effect of each producer-cell gene knockout on eVLP
110 production or cargo loading (Fig. 1b and Extended Data Fig. 1c). We observed that the
111 majority of gene knockouts did not substantially impact eVLP production or cargo loading,
112 some knockouts decreased eVLP production or cargo loading, and very few knockouts
113 increased eVLP production or cargo loading (Fig. 1b). These results are consistent with
114 a model in which there are more genes in producer cells that positively regulate eVLP
115 production than genes that negatively regulate eVLP production. Taken together, the
116 results of this genome-wide knockout screen illuminate the producer-cell determinants of
117 eVLP production and nominate several gene knockouts ("hits") that appear to strongly
118 impact eVLP production or cargo loading (Fig. 1b).
119

120 *Knockout of HUSH-associated genes negatively impacts eVLP sgRNA packaging in the*
121 *presence of lentiviral Cas9 expression*
122 Next, we sought to characterize the gene knockouts that most strongly decreased
123 eVLP production or cargo loading. While these negative hits might not be immediately
124 applicable for improving eVLP manufacturing, we reasoned that characterizing these
125 gene knockouts would reveal important insights into how producer-cell factors influence
126 eVLPs, which could inform alternative strategies for improving eVLP production. The
127 three strongest negative hits from our screen—*MPP8*, *TASOR*, and *MORC2*—are all
128 associated with the human silencing hub (HUSH) complex, which is responsible for
129 epigenetically silencing intronless transgenes, including retroviral elements[32,33]. We first
130 individually validated each negative hit by measuring the relative sgRNA abundance in
131 eVLPs produced from *MPP8*-, *TASOR*-, or *MORC2*-knockout cells (hereafter collectively
132 referred to as HUSH-knockout cells) compared to eVLPs produced from standard
133 producer cells. To independently generate each knockout cell line, we mimicked the
134 screen conditions and transduced Gesicle cells with a lentiviral vector encoding
135 constitutive expression of Cas9 nuclease and an appropriate targeting sgRNA, selected
136 cells for Cas9 expression, and isolated a polyclonal population of Cas9-edited cells
137 (Extended Data Fig. 2a). To control for the effects of Cas9 expression and Cas9 nuclease-
138 mediated indel generation on producer cells, we also applied the same procedure to
139 generate modified Gesicle cells using a sgRNA targeting *AAVS1*, a human safe harbor
140 locus[34]. After knockout generation, we initiated v4 ABE-eVLP production from each cell
141 line by transfecting plasmids encoding the expression of all required components,
142 including a sgRNA targeting the human *BCL11A* +58 enhancer locus[35] (Extended Data
143 Fig. 2a). We detected by RT-qPCR a 1.5- to 3.8-fold decrease in sgRNA abundance in
144 ABE-eVLPs produced from HUSH-knockout cells compared to ABE-eVLPs produced
145 from *AAVS1*-knockout cells (Fig. 2a), confirming the results of our screen. Additionally,
146 when we transduced HEK293T cells with a range of doses of purified ABE-eVLPs and
147 measured adenine base editing efficiencies at the *BCL11A* +58 enhancer target locus via
148 high-throughput sequencing (Extended Data Fig. 2a), we observed that ABE-eVLPs
149 produced from HUSH-knockout cells exhibited a 2.3- to 4.4-fold decrease in *in vitro*
150 delivery potency (EC_{50}) compared to ABE-eVLPs produced from *AAVS1*-knockout cells

151 (Fig. 2b). These results indicate that knockout of HUSH-associated genes *MPP8*, *TASOR*,
152 or *MORC2* in producer cells negatively impacts eVLP production or cargo loading.
153 We hypothesized that these HUSH-associated genes might impact eVLP
154 production or cargo loading by modulating the expression of the lentivirally integrated
155 Cas9 nuclease that was used to generate the gene knockouts. To test this hypothesis,
156 we measured the relative abundance of Cas9 mRNA or protein in each knockout cell line
157 by RT-qPCR or Western blot respectively. We observed a 5.4- to 29-fold increase in
158 cellular Cas9 mRNA expression and a 10- to 14-fold increase in Cas9 protein expression
159 in HUSH-knockout cells compared to *AAVS1*-knockout cells (Fig. 2c, d and Extended
160 Data Fig. 3a). These results suggest a model in which HUSH-associated gene products
161 natively silence lentivirally integrated Cas9 expression in *AAVS1*-knockout producer cells,
162 but in HUSH-knockout cells, Cas9 is no longer efficiently silenced (Extended Data Fig.
163 3b). Therefore, during eVLP production, excess Cas9 protein in HUSH-knockout producer
164 cells likely competes for sgRNA binding and prevents sgRNA molecules from efficiently
165 binding to gag–ABE, which ultimately decreases both sgRNA packaging into eVLPs and
166 eVLP delivery potency (Extended Data Fig. 3b). To further investigate this phenomenon,
167 we used v4 Cas9-eVLP transduction instead of Cas9/sgRNA lentiviral transduction to
168 generate HUSH-knockout Gesicle cells that lacked any integrated Cas9 transgene
169 (Extended Data Fig. 2b). Notably, we did not detect any change in sgRNA abundance by
170 RT-qPCR in ABE-eVLPs produced from these Cas9-free HUSH-knockout cells compared
171 to standard producer cells (Extended Data Fig. 4a). These results suggest that, consistent
172 with our model above, both lentivirally integrated Cas9 expression and knockout of
173 HUSH-associated genes are required to decrease sgRNA abundance in eVLPs.
174 Collectively, these data and our proposed model rationalize the negative performance of
175 HUSH-associated gene knockouts in our screen.
176
177 *Knockout of HUSH-associated genes increases eVLP protein cargo expression*
178 Interestingly, we noticed that ABE-eVLPs produced from Cas9-free HUSH-
179 knockout cells still exhibited a 2.6- to 3.9-fold decrease in delivery potency compared to
180 ABE-eVLPs produced from standard Gesicle cells (Extended Data Fig. 4b), suggesting
181 that some eVLP property other than sgRNA abundance was negatively impacted due to

182 Cas9-free HUSH-associated gene knockout. We hypothesized that these HUSH-
183 associated genes might also modulate the expression of eVLP components from
184 plasmids transfected during the eVLP production process. To investigate this possibility,
185 we performed Western blots to quantify eVLP cargo (gag–ABE) expression in producer
186 cells following transfection of eVLP production plasmids, which revealed a 2.1- to 4.4-fold
187 increase in gag–ABE protein expression in HUSH-knockout cells compared to Gesicle
188 cells (Extended Data Fig. 4c, d). We reasoned that this increase in eVLP cargo expression
189 might disrupt the optimal eVLP component stoichiometry (gag–ABE:gag–pro–pol ratio),
190 which was previously found to be an important determinant of eVLP potency[8]. Consistent
191 with this model, we observed that reducing the transfected gag–ABE:gag–pro–pol
192 plasmid ratio from 25:75 to 10:90 or 5:95 restored the potency of ABE-eVLPs produced
193 from *MORC2*-knockout cells back to standard levels (Extended Data Fig. 4e). These
194 results indicate that the increase in eVLP cargo expression in HUSH-knockout producer
195 cells and corresponding disruption of the optimal eVLP component stoichiometry can be
196 counteracted simply by reducing the amount of transfected eVLP cargo plasmid, thereby
197 effectively restoring the optimal stoichiometry.

198 Given our finding that knockout of HUSH-associated genes increases eVLP cargo
199 expression, we wondered whether HUSH-knockout producer cells could in fact improve
200 eVLP production in specific contexts. In particular, certain applications of eVLPs,
201 including our recently described barcoded eVLP evolution system[22], require expressing
202 gag–ABE from genomically integrated cassettes rather than transfected plasmids, which
203 results in reduced gag–ABE protein levels and suboptimal component stoichiometry. We
204 reasoned that the use of HUSH-knockout producer cells should increase gag–ABE
205 expression from genomically integrated cassettes, which in this case would improve
206 rather than disrupt the eVLP component stoichiometry (Fig. 2e). Consistent with this
207 model, we observed that ABE-eVLPs produced from *MORC2*-knockout cells with
208 integrated gag–ABE expression exhibited a 4.6-fold increase in delivery potency
209 compared to ABE-eVLPs produced from standard cells with integrated gag–ABE
210 expression (Fig. 2f). These results indicate that HUSH-knockout producer cells support
211 improved eVLP delivery potency in situations in which gag–cargo expression is limiting.
212 Altogether, our results reveal a previously unknown role for HUSH-associated genes in

213 modulating eVLP cargo expression in producer cells and highlight the importance of
214 optimizing eVLP cargo expression and component stoichiometry to maximize eVLP
215 potency.
216
217 *MAF1-knockout producer cells improve sgRNA packaging into eVLPs*
218 Next, we sought to characterize the gene knockouts from our screen that most
219 strongly increased eVLP production or cargo loading. The single strongest positive hit
220 from our screen was *MAF1*, a repressor of RNA Pol III transcription[36-38]. Because all
221 sgRNAs in our experiments were expressed from an RNA Pol III-transcribed U6 promoter,
222 we reasoned that knockout of *MAF1* in producer cells likely leads to increased sgRNA
223 transcription and loading into eVLP-packaged cargos (Fig. 3a).
224 To test this hypothesis, after generating *MAF1*-knockout Gesicle cells using v4
225 Cas9-eVLPs (Extended Data Fig. 2b), we initiated v4 ABE-eVLP production from these
226 cells by transfecting plasmids encoding the expression of all required components. We
227 detected by RT-qPCR a 2-fold increase in sgRNA abundance in ABE-eVLPs produced
228 from *MAF1*-knockout cells compared to ABE-eVLPs produced from standard Gesicle
229 cells (Fig. 3b). Additionally, we observed that ABE-eVLPs produced from *MAF1*-knockout
230 cells were produced at similar particle titers and packaged similar numbers of ABE cargo
231 proteins per particle compared to ABE-eVLPs produced from standard Gesicle cells (Fig.
232 3c, d), suggesting that the use of *MAF1*-knockout cells increases sgRNA packaging alone
233 without affecting protein packaging or particle yield. Collectively, these data confirm our
234 knockout screen results and indicate that *MAF1*-knockout producer cells support
235 increased sgRNA loading into eVLPs.
236
237 *MAF1-knockout producer cells support improved eVLP delivery potency in cell culture*
238 *and in mice*
239 Because increased sgRNA loading leads to an increased number of active RNP
240 cargo molecules packaged into eVLPs (Fig. 3a), we reasoned that ABE-eVLPs produced
241 from *MAF1*-knockout cells should exhibit increased delivery potency compared to ABE-
242 eVLPs produced from standard Gesicle cells. Encouragingly, we observed that v4 ABE-
243 eVLPs produced from *MAF1*-knockout cells exhibited a 2.5-fold increase in delivery

244 potency (EC_{50}) at the *BCL11A* +58 enhancer locus in HEK293T cells compared to v4
245 ABE-eVLPs produced from standard Gesicle cells (Fig. 4a). v4 ABE-eVLPs produced
246 from *MAF1*-knockout cells also exhibited a 2.2- and 2.1-fold increase in delivery potency
247 at the *GAPDH* and *HIRA* genomic loci in HEK293T cells, respectively (Fig. 4b, c),
248 indicating that the eVLP potency improvement conferred by the use of *MAF1*-knockout
249 producer cells is not restricted to any particular sgRNA sequence or target genomic locus.
250 Additionally, we assessed whether the use of *MAF1*-knockout producer cells could also
251 improve the delivery potency of the more recently developed v5 ABE-eVLPs, which use
252 laboratory evolved capsid proteins that were optimized to improve BE RNP cargo
253 packaging[22]. We observed that v5 ABE-eVLPs produced from *MAF1*-knockout cells
254 exhibited a 2.2- to 9.1-fold increase in delivery potency compared to v5 ABE-eVLPs
255 produced from standard cells across six distinct target genomic loci in mouse Neuro-2a
256 cells (Fig. 4d–i). Together, these results indicate that the increased sgRNA packaging in
257 ABE-eVLPs produced from *MAF1*-knockout cells leads to corresponding improvements
258 in eVLP delivery potency *in vitro*.
259 To further explore the utility of *MAF1*-knockout producer cells, we investigated
260 whether their use could also improve *in vivo* eVLP delivery efficiencies. We produced v5
261 ABE-eVLPs targeting the *Pcsk9* exon 1 splice donor[8,39] using either standard or *MAF1*-
262 knockout Gesicle cells, and we injected these ABE-eVLPs retro-orbitally into adult mice
263 at a low, sub-saturating eVLP dose (Fig. 4j). We observed that v5 ABE-eVLPs produced
264 from *MAF1*-knockout cells achieved 19.4% average *in vivo* base editing at the *Pcsk9*
265 locus in bulk liver tissue, while v5 ABE-eVLPs produced from standard cells administered
266 at the same dose only achieved 12.6% bulk liver editing (Fig. 4j, $P = 0.0365$, two-sided
267 unpaired *t* test). Collectively, these data indicate that *MAF1*-knockout producer cells
268 support improved eVLP potency across different target genomic loci and target-cell types
269 both *in vitro* and *in vivo*, demonstrating the benefits of using *MAF1*-knockout cells instead
270 of standard cells for eVLP production.
271
272 *MAF1-knockout producer cells support improved delivery potency across various cargo,*
273 *particle, and producer-cell types*

274 We next sought to further evaluate the ability of *MAF1*-knockout producer cells to
275 support improved eVLP production and potency in other various contexts. First, we
276 investigated whether knockout of *MAF1* could improve eVLP production from
277 HEK293T/17 cells, another cell line that is commonly used for viral vector production[8,22,40].
278 Following the generation of *MAF1*-knockout HEK293T/17 cells using v4 Cas9-eVLPs, we
279 observed that v4 ABE-eVLPs produced from *MAF1*-knockout HEK293T/17 cells exhibited
280 a 2.5-fold increase in *in vitro* delivery potency compared to those produced from standard
281 HEK293T/17 cells (Fig. 4k). These results indicate that the improvements conferred by
282 *MAF1* knockout are generalizable beyond the specific cell line (Gesicle 293T) in which
283 our knockout screen was conducted. Additionally, our findings suggest that knockout of
284 *MAF1* might similarly benefit eVLP production from HEK293T/17 clones that have been
285 adapted for growth in suspension culture, which are particularly well suited for large-scale
286 bioparticle manufacturing[41].
287 Second, we assessed whether *MAF1*-knockout producer cells could improve the
288 potency of eVLPs that package different Cas9-based RNP cargos. We observed that v4
289 eVLPs packaging either Cas9 nuclease, ABE-SpCas9-NG[42], or TadCBEa[43] cargos
290 exhibited a 2.0- to 2.5-fold improvement in delivery potency when produced from *MAF1*-
291 knockout cells compared to Gesicle cells (Fig. 5a–e).
292 Third, we explored whether *MAF1*-knockout producer cells could also improve the
293 performance of non-eVLP delivery vehicles, including several recently reported RNP-
294 packaging VLP- and vesicle-based systems. We evaluated four different non-eVLP
295 systems that use various particle scaffolds and cargo loading mechanisms (Extended
296 Data Fig. 5a): (1) ENVLPE$^+$ (engineered nucleocytosolic vehicles for loading of
297 programmable editors)[10], (2) miniEDV (minimal enveloped delivery vehicles)[44], (3) RIDE
298 VLPs[16], and (4) VEDIC (VSV-G plus EV-Sorting Domain-Intein-Cargo)[45] particles. We
299 observed that ABE-packaging ENVLPE$^+$ particles produced from *MAF1*-knockout cells
300 exhibited a 2.2-fold increase in delivery potency compared to the same particles produced
301 from standard Gesicle cells, which was nearly identical to the improvement we observed
302 for v4 ABE-eVLPs (Extended Data Fig. 5b, c). Prime editor (PE)-packaging ENVLPE$^+$
303 particles produced from *MAF1*-knockout cells also exhibited a 2.1-fold increase in delivery
304 potency compared to the same particles produced from standard Gesicle cells (Extended

305 Data Fig. 5d). Additionally, we observed that Cas9-packaging miniEDVs, ABE-packaging
306 RIDE VLPs, and Cas9-packaging VEDIC particles produced from *MAF1*-knockout cells
307 exhibited a 1.7-, 1.8-, and 2.6-fold increase in delivery potency, respectively, compared
308 to the same particles produced from standard Gesicle cells (Extended Data Fig. 5e–g).
309 These results indicate that the improvements conferred by *MAF1*-knockout producer cells
310 are generalizable across several different RNP-packaging cell-derived bioparticles that
311 use distinct particle scaffolds and cargo packaging mechanisms. Taken together, our
312 findings demonstrate that knockout of *MAF1* in producer cells yields consistent
313 improvements in VLP delivery potency across eVLP cargo types, particle types, and
314 producer-cell lines.
315
316 *MAF1-knockout producer cells improve sgRNA packaging into eVLPs across different*
317 *sgRNA expression levels*
318 Finally, we evaluated whether the improvements conferred by *MAF1*-knockout
319 cells could synergize with additional strategies for modulating sgRNA expression levels
320 in producer cells. We observed that increasing the ratio of sgRNA-expressing plasmid to
321 other packaging plasmids transfected during eVLP production did not improve the
322 delivery potency of v4 ABE-eVLPs produced from either standard Gesicle cells or *MAF1*-
323 knockout cells (Extended Data Fig. 6a, b). Increasing the absolute amount of sgRNA-
324 expressing plasmid transfected during eVLP production by up to two-fold also did not
325 improve the delivery potency of v4 ABE-eVLPs produced from either standard Gesicle
326 cells or *MAF1*-knockout cells (Extended Data Fig. 6c). These results indicate that simply
327 increasing the amount of sgRNA-expressing plasmid transfected during eVLP production
328 is not sufficient to improve eVLP potency, possibly because of tradeoffs associated with
329 either reducing the amounts of other packaging plasmids or increasing the total amount
330 of transfected DNA per producer cell.
331 To further investigate alternative strategies for improving sgRNA expression, we
332 adopted a strategy that was recently developed for EDVs in which additional sgRNA
333 expression cassettes are included in the other packaging plasmids[13] (Extended Data Fig.
334 7a). This strategy (hereafter referred to as ++sgRNA) avoids the tradeoffs mentioned
335 above since the amount of sgRNA-encoding DNA is increased without substantially

336 perturbing the amounts of other packaging plasmids or the total amount of transfected
337 DNA per producer cell. We observed that v4 ABE-eVLPs produced from Gesicle cells
338 using ++sgRNA plasmids exhibited a 3.3-fold increase in delivery potency compared to
339 standard v4 ABE-eVLPs produced from Gesicle cells (Fig. 5f). Additionally, we observed
340 that v4 ABE-eVLPs produced from *MAF1*-knockout cells using ++sgRNA plasmids also
341 exhibited a 3.4-fold increase in delivery potency compared to standard v4 ABE-eVLPs
342 produced from *MAF1*-knockout cells (Fig. 5f). These results indicate that the use of
343 ++sgRNA plasmids synergizes with *MAF1*-knockout producer cells to further improve
344 delivery potency. Importantly, v4 ABE-eVLPs produced using ++sgRNA plasmids still
345 exhibited a 2.6-fold increase in delivery potency when produced from *MAF1*-knockout
346 cells compared to Gesicle cells, highlighting the consistent benefit of using *MAF1*-
347 knockout producer cells. Indeed, combining ++sgRNA plasmids and *MAF1*-knockout
348 producer cells yielded the most potent eVLP-mediated base editing at the *BCL11A*
349 enhancer site in HEK293T cells that we observed in this study (Fig. 5f).
350 We confirmed via RT-qPCR that both the ++sgRNA strategy and knockout of
351 *MAF1* led to increased sgRNA packaging into eVLPs; these increases in sgRNA
352 packaging were additive when both modified strategies were employed (Extended Data
353 Fig. 7b). In particular, we observed that combining both strategies increased the
354 percentage of eVLP-packaged Cas9 molecules complexed with sgRNAs from 20% to 50%
355 (Extended Data Fig. 7b). Collectively, our findings demonstrate that the use of *MAF1*-
356 knockout producer cells can further improve eVLP properties when combined with
357 additional strategies for increasing sgRNA expression during eVLP production.
358
359 **Discussion**
360 In this study, we developed a general genome-wide screening approach to
361 comprehensively evaluate how genetic perturbations in producer cells influence eVLP
362 production. Using this approach, we identified the HUSH epigenetic silencing complex
363 and the RNA Pol III repressor MAF1 as key regulators of eVLP protein and sgRNA cargo
364 expression, respectively. Leveraging these insights, we engineered HUSH-knockout
365 producer cells that support a 4-fold increase in eVLP delivery potency when particles are
366 produced using genomically integrated gag–cargo expression, and *MAF1*-knockout

367 producer cells that support a 2- to 9-fold increase in eVLP delivery potency under
368 standard production conditions across several cargo, particle, producer-cell, and target-
369 cell types.

370 Our results reveal a previously underappreciated role for the HUSH complex in
371 modulating eVLP protein cargo expression in producer cells. Under standard eVLP
372 production conditions, we found that HUSH-knockout producer cells exhibited increased
373 gag–cargo expression, which disrupted the optimal component stoichiometry and
374 reduced eVLP potency. However, under conditions in which gag–cargo expression is
375 limiting, including when particles are produced using genomically integrated gag–cargo
376 expression, we found that the use of HUSH-knockout producer cells improved eVLP
377 delivery potency (Fig. 2f). We therefore anticipate that HUSH-knockout producer cells will
378 be useful for eVLP applications in which genomically integrated gag–cargo expression is
379 required (e.g. barcoded eVLP evolution[22]). Additionally, our results suggest that HUSH-
380 knockout cells are likely to be valuable for future efforts to produce eVLPs or related
381 particles using producer cells that stably express components from genomically
382 integrated cassettes instead of transfected plasmids, a strategy that has proven useful
383 for viral vector manufacturing[27,46-48].

384 We anticipate that the use of *MAF1*-knockout cells instead of standard producer
385 cells will advance the utility of VLP delivery in several ways. For one, eVLPs produced
386 from *MAF1*-knockout cells exhibit increased sgRNA packaging and increased delivery
387 potency both in cell culture and in mice compared to standard eVLPs (Fig. 4), suggesting
388 that *MAF1*-knockout producer cells should be used when maximal editing efficiencies are
389 required. Additionally, the gene editing efficiencies at a given dose of eVLPs produced
390 from standard cells can in general be achieved using a 2- to 9-fold lower dose of eVLPs
391 produced from *MAF1*-knockout cells (Fig. 4a–i), suggesting that using *MAF1*-knockout
392 cells for eVLP production will be especially beneficial for applications that are constrained
393 by the maximum administrable eVLP dose. Furthermore, by minimizing the eVLP dose
394 required to achieve efficient editing, the use of *MAF1*-knockout producer cells would also
395 reduce the total volume of producer-cell culture required for eVLP production, which could
396 greatly simplify the application of eVLPs in large-scale studies. Importantly, given that
397 several previous studies have identified sgRNA loading into VLPs and related delivery

398 vehicles as a bottleneck that limits delivery potency[8,13,22,49], our discovery that *MAF1*-
399 knockout producer cells improve sgRNA loading into VLPs will likely be widely applicable
400 for improving RNP delivery using various cell-derived bioparticles, including the five
401 distinct VLP constructs we tested in this study (Extended Data Fig. 5).

402 Altogether, our study provides a general workflow for identifying perturbations in
403 producer cells that impact eVLP production and genetically engineering producer cells for
404 improved eVLP production. While previous studies have applied CRISPR screens that
405 use particle-packaged nucleic acid as a way to investigate the cellular determinants of
406 viral vector[24-26] or extracellular vesicle production[50,51], our study is the first to our
407 knowledge that leverages insights from a producer-cell screen to improve VLP production
408 and delivery potency. Notably, our results highlight the importance of conducting a
409 producer-cell screen using RNP-packaging VLPs instead of viral vectors, since we
410 uncovered genes that are uniquely relevant for RNP cargo expression and packaging.
411 Additionally, our screen design is highly general and can be applied to evaluate various
412 genetic and epigenetic perturbations on a genome-wide scale, including for CRISPR
413 activation or base editing screens. We anticipate that further improvements in particle
414 production are likely possible by employing varied producer-cell perturbations instead of
415 single gene knockouts alone. Overall, while iterative particle architecture engineering
416 continues to improve VLP delivery potency and cell-type targeting capabilities[10,13,22,52],
417 our work establishes producer-cell genetic engineering as a distinct and potentially
418 powerful strategy for maximizing the utility of VLP-based delivery modalities.

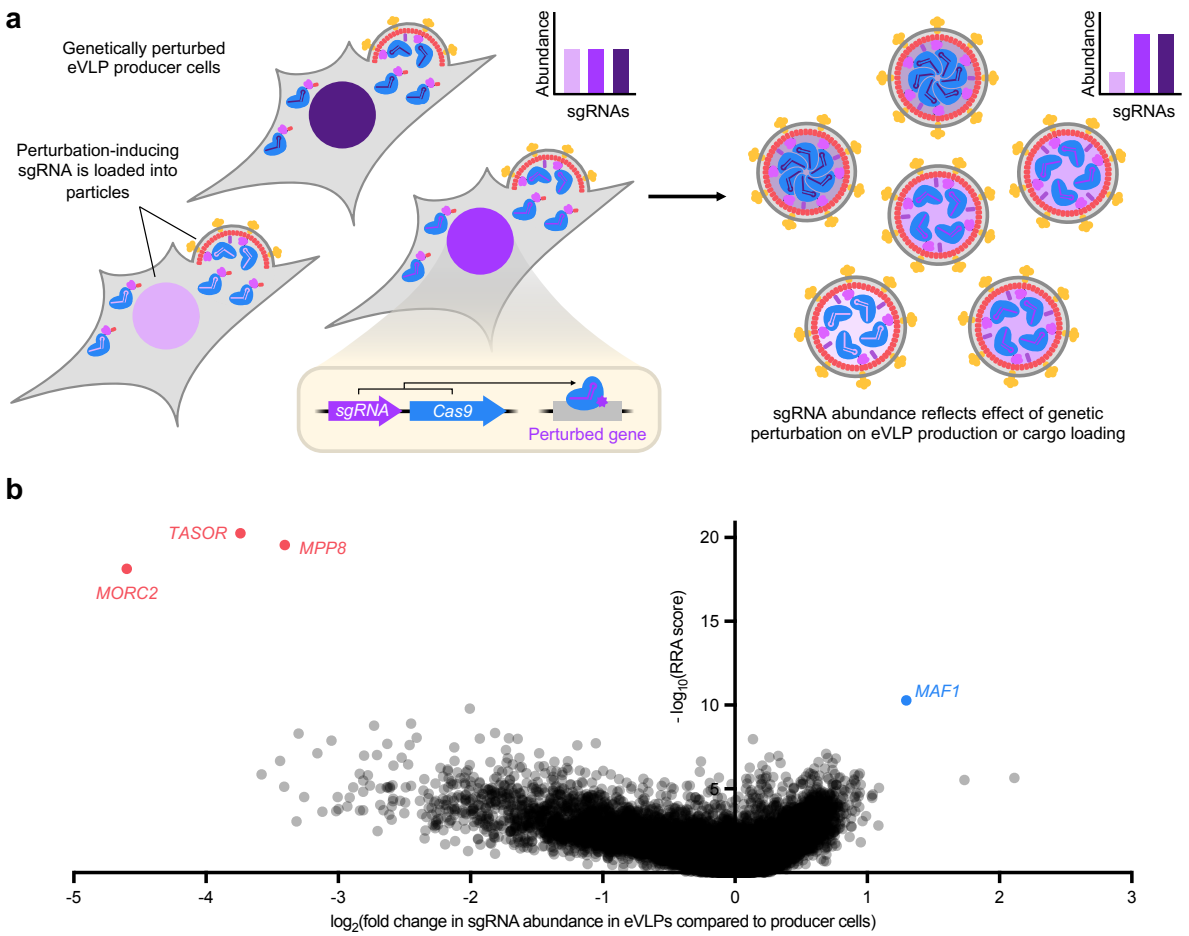

Fig. 1 | Genome-wide screening reveals genetic perturbations that influence eVLP production. a, Overview of the producer-cell screening approach. eVLP production is initiated from a pool of genetically perturbed producer cells, and each eVLP packages sgRNAs that identify the specific genetic perturbation in the cell that produced that particular eVLP. The abundance of a particular sgRNA in eVLPs compared to producer cells reflects how the corresponding genetic perturbation influences eVLP production or cargo loading. **b**, Gene-level phenotypes from the genome-wide knockout screen for cargo-loaded eVLP production. Each gene is represented as a single dot whose x-coordinate reflects the median fold change in sgRNA abundance in eVLPs compared to producer cells for all sgRNAs targeting that particular gene, and whose y-coordinate reflects the MAGeCK RRA score associated with that particular gene (see Methods). Data reflect n=2 screen replicates. See also Extended Data Fig. 1c and Supplementary Table 6.

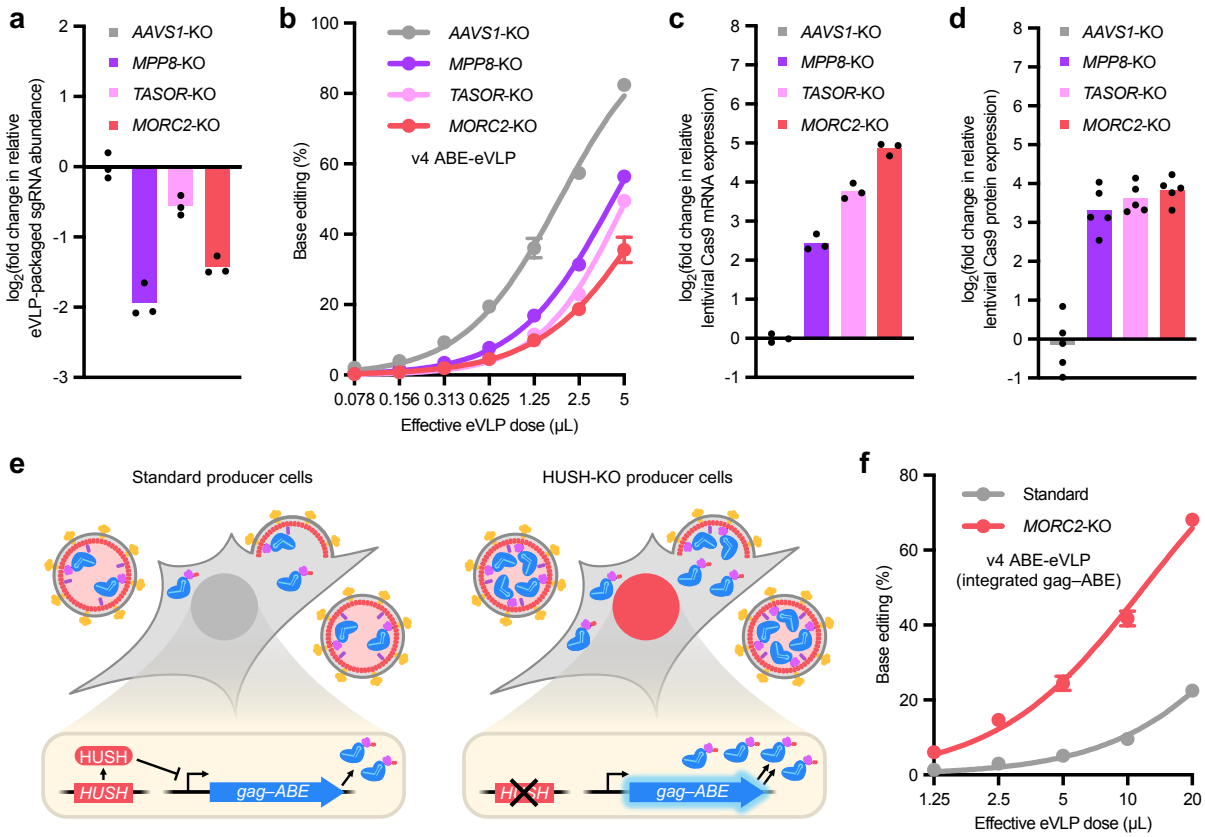

Fig. 2 | Knockout of HUSH-associated genes negatively impacts eVLP sgRNA packaging and delivery potency. a, Fold change in eVLP-packaged sgRNA abundance measured by RT-qPCR, normalized relative to sgRNA abundance in eVLPs produced from *AAVS1*-knockout cells. Bars reflect the mean of n=3 replicates, and dots represent individual replicate values. **b**, Comparison of v4 ABE-eVLPs produced from *AAVS1*-knockout or HUSH-knockout cells across a range of eVLP doses. Adenine base editing efficiencies at position A_7 of the *BCL11A* +58 enhancer site in HEK293T cells are shown. **c**, Fold change in producer-cell Cas9 mRNA abundance measured by RT-qPCR, normalized relative to Cas9 mRNA abundance in *AAVS1*-knockout cells. Bars reflect the mean of n=3 replicates, and dots represent individual replicate values. **d**, Fold change in producer-cell Cas9 protein abundance measured by Western blot, normalized relative to Cas9 protein abundance in *AAVS1*-knockout cells. Bars reflect the mean of n=5 replicates, and dots represent individual replicate values. See also Extended Data Fig. 3a. **e**, Schematic of standard producer cells versus HUSH-knockout producer cells, both containing genomically integrated gag–ABE expression cassettes. In standard cells, epigenetic silencing by the HUSH complex limits gag–ABE expression. In HUSH-knockout cells, lack of HUSH-mediated silencing leads to increased gag–ABE expression and loading into eVLPs. **f**, Comparison of v4 ABE-eVLPs produced from standard or *MORC2*-knockout Gesicle cells, both containing genomically integrated gag–ABE expression cassettes. Adenine base editing efficiencies at position A_5 of the *HEK2* site in HEK293T cells are shown. In **b** and **f**, dots and error bars represent mean ± s.d. of n=3 biological replicates. Data were fit to four-parameter logistic curves using nonlinear regression.

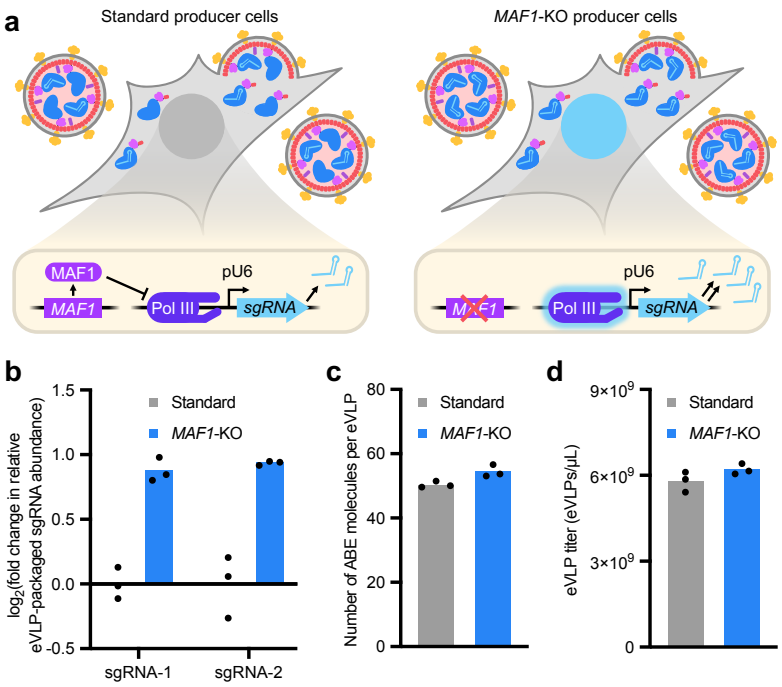

Fig. 3 | *MAF1*-knockout producer cells improve eVLP sgRNA packaging. a, Schematic of standard producer cells versus *MAF1*-knockout producer cells. In standard cells, MAF1 represses RNA Pol III transcription, which limits producer-cell sgRNA expression. In *MAF1*-knockout producer cells, RNA Pol III is no longer subjected to MAF1-mediated repression, which increases sgRNA expression and loading into eVLP-packaged RNPs. **b**, Fold change in eVLP-packaged sgRNA abundance measured by RT-qPCR, normalized relative to sgRNA abundance in eVLPs produced from standard Gesicle cells. sgRNA-1 and sgRNA-2 denote two different packaged sgRNA sequences. **c–d**, Quantification of ABE molecules per eVLP (**c**) and eVLP particle titer (**d**) by anti-Cas9 and anti-MLV p30 ELISA (see Methods). In **b–d**, bars reflect the mean of n=3 replicates, and dots represent individual replicate values.

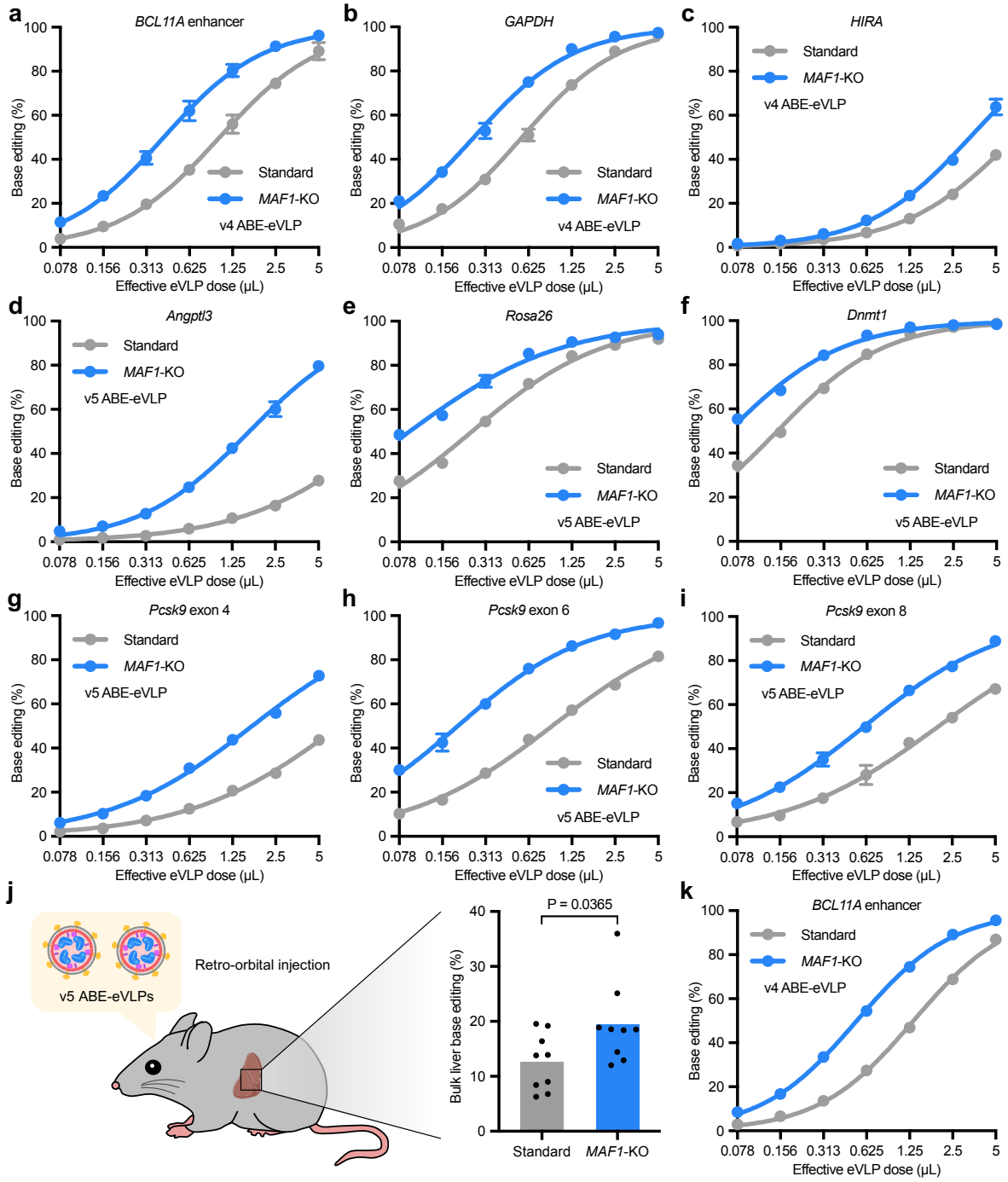

Fig. 4 | *MAF1*-knockout producer cells improve eVLP delivery potency in cultured cells and in mice. a–c, Comparison of v4 ABE-eVLPs produced from standard or *MAF1*-knockout Gesicle cells across a range of eVLP doses in HEK293T cells. Adenine base editing efficiencies are shown at position A_7 of the *BCL11A* +58 enhancer site (**a**), position A_7 of the *GAPDH* site (**b**), and position A_5 of the *HIRA* site (**c**). **d–i**, Comparison of v5 ABE-eVLPs produced from standard or *MAF1*-knockout Gesicle cells across a range of eVLP doses in mouse Neuro-2a cells. Adenine base editing efficiencies are shown at position A_8 of the *Angptl3* exon 7 splice acceptor site (**d**), position A_4 of the *Rosa26* site

(**e**), position A_9 of the *Dnmt1* site (**f**), position A_6 of the *Pcsk9* exon 4 splice acceptor site (**g**), position A_4 of the *Pcsk9* exon 6 splice donor site (**h**), and position A_8 of the *Pcsk9* exon 8 splice acceptor site (**i**). **j**, Schematic of mouse experiments and adenine base editing efficiencies at position A_6 of the *Pcsk9* exon 1 splice donor site in bulk mouse liver tissue. Each mouse was injected with 15 µL of 1500-fold concentrated purified v5 ABE-eVLPs containing 3×10^{11} eVLPs as determined by anti-MLV p30 ELISA (see Methods). Bars reflect the mean of n=9 mice per condition, and dots represent individual mouse values. P-value was calculated using a two-sided unpaired t test. **k**, Comparison of v4 ABE-eVLPs produced from standard or *MAF1*-knockout HEK293T/17 cells across a range of eVLP doses in HEK293T cells. Adenine base editing efficiencies at position A_7 of the *BCL11A* +58 enhancer site are shown. In **a–i** and **k**, dots and error bars represent mean ± s.d. of n=4 (**a**) or n=3 (**b–i**, **k**) biological replicates. Data were fit to four-parameter logistic curves using nonlinear regression.

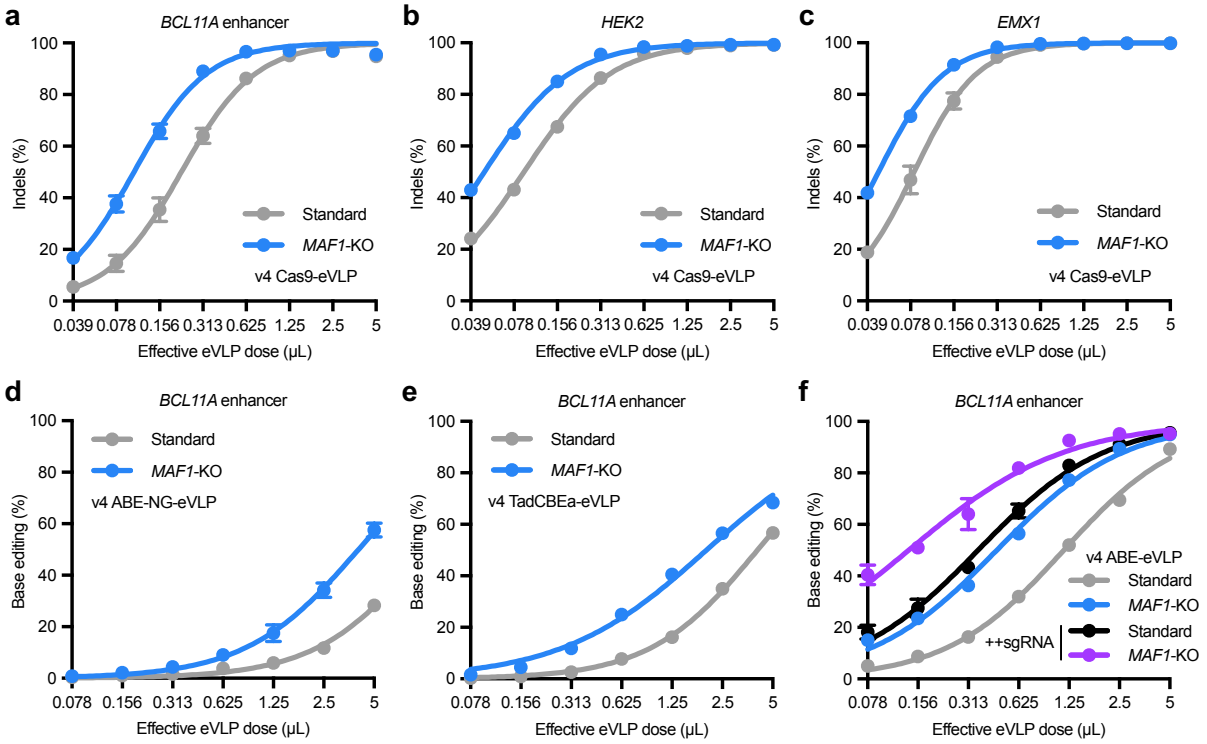

Fig. 5 | *MAF1*-knockout producer cells improve eVLP delivery potency across cargo types. a–c, Comparison of v4 Cas9-eVLPs produced from standard or *MAF1*-knockout Gesicle cells across a range of eVLP doses in HEK293T cells. Indel frequencies are shown at the *BCL11A* +58 enhancer site (**a**), *HEK2* site (**b**), and *EMX1* site (**c**). **d**, Comparison of v4 ABE-NG-eVLPs produced from standard or *MAF1*-knockout Gesicle cells across a range of eVLP doses. Adenine base editing efficiencies at position A_7 of the *BCL11A* +58 enhancer site in HEK293T cells are shown. **e**, Comparison of v4 TadCBEa-eVLPs produced from standard or *MAF1*-knockout Gesicle cells across a range of eVLP doses. Cytosine base editing efficiencies at position C_6 of the *BCL11A* +58 enhancer site in HEK293T cells are shown. **f**, Comparison of v4 ABE-eVLPs or v4 ABE-eVLPs with additional sgRNA-expressing plasmids (++sgRNA, see Extended Data Fig. 7) produced from standard or *MAF1*-knockout Gesicle cells across a range of eVLP doses. Adenine base editing efficiencies at position A_7 of the *BCL11A* +58 enhancer site in HEK293T cells are shown. **a–f**, Dots and error bars represent mean ± s.d. of n=3 biological replicates. Data were fit to four-parameter logistic curves using nonlinear regression.

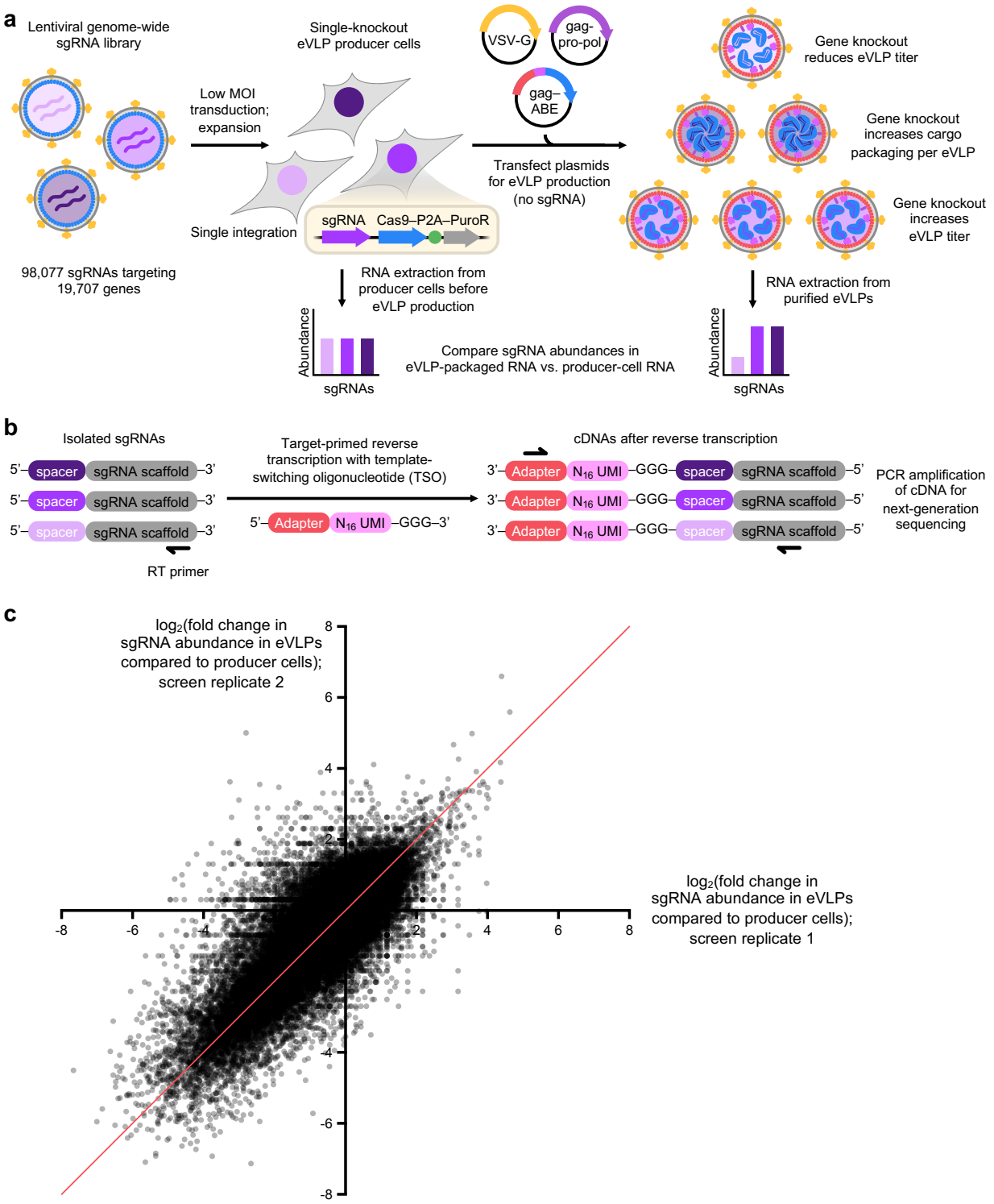

Extended Data Fig. 1 | Genome-wide knockout screening for cargo-loaded eVLP production. a, Overview of the genome-wide knockout screening approach. Low-MOI Cas9/sgRNA lentiviral transduction was used to introduce a genome-wide sgRNA library into Gesicle producer cells, thereby generating a pool of single-knockout producer cells. eVLP production was then initiated from this pool by transfecting expressing eVLP protein

513 components. No additional sgRNA-encoding plasmid was transfected, ensuring that all
514 eVLPs produced from a given producer cell packaged cargo containing the specific
515 knockout-inducing sgRNA that was already introduced into that producer cell by lentiviral
516 transduction. The abundance of a particular sgRNA in eVLPs compared to producer cells
517 reflects how the corresponding gene knockout influences eVLP production or cargo
518 loading. **b**, Schematic of the template-switching reverse transcription approach used for
519 direct-capture sgRNA spacer sequencing from both eVLP-packaged RNA and producer-
520 cell RNA. UMI=unique molecular identifier. **c**, Fold change in sgRNA abundance in eVLPs
521 compared to producer cells across replicates of the genome-wide knockout screen. Each
522 sgRNA in the library is represented as a single dot and reflects the values from n=2 screen
523 replicates. The y=x line is plotted in red. See also Supplementary Tables 3–5.

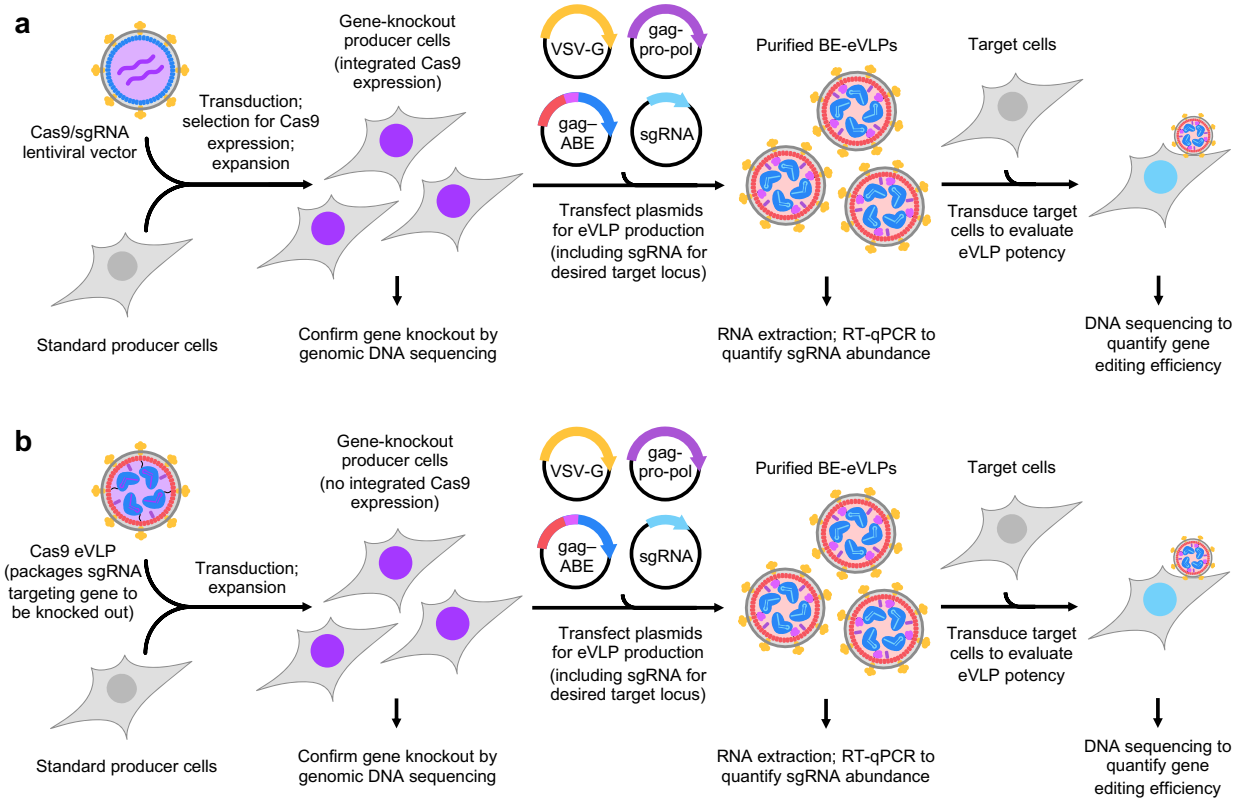

Extended Data Fig. 2 | Generating and characterizing single-knockout producer cell lines. a, Schematic of generating polyclonal single-knockout producer cells via Cas9/sgRNA lentiviral transduction, followed by characterizing the resulting cell lines and their use for eVLP production. **b**, Schematic of generating polyclonal single-knockout producer cells via v4 Cas9-eVLP transduction, followed by characterizing the resulting cell lines and their use for eVLP production.

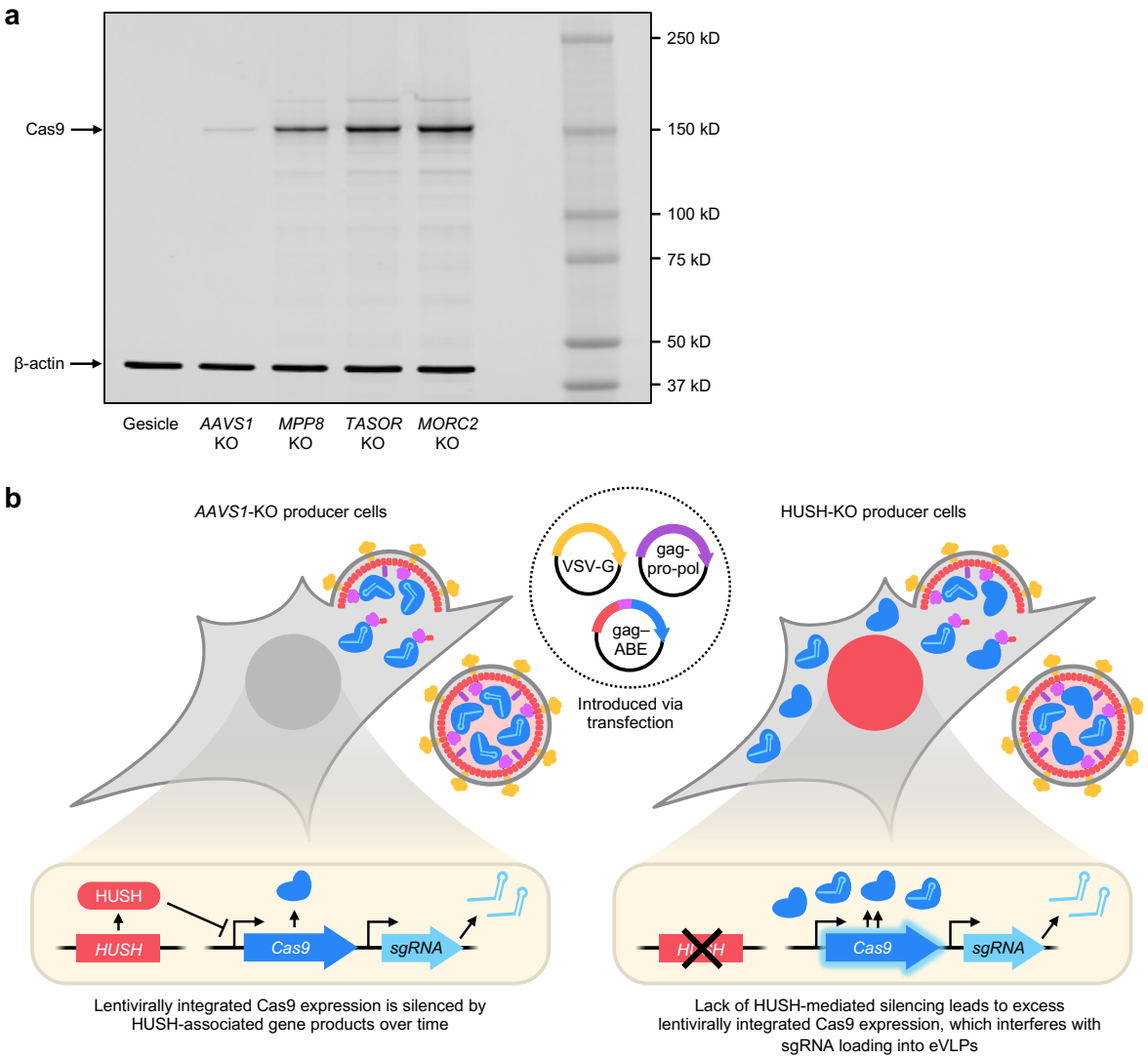

Extended Data Fig. 3 | HUSH-knockout producer cells exhibit increased lentiviral Cas9 expression. a, Western blot analysis of producer-cell protein lysates. **b**, Proposed model for *AAVS1*-knockout producer cells versus HUSH-knockout producer cells. In *AAVS1*-knockout cells, HUSH-associated gene products silence lentivirally integrated Cas9 expression over time. In HUSH-knockout producer cells, lack of HUSH-mediated silencing leads to excess expression of lentivirally integrated Cas9, which interferes with sgRNA loading into eVLPs and therefore reduces eVLP-packaged sgRNA abundance.

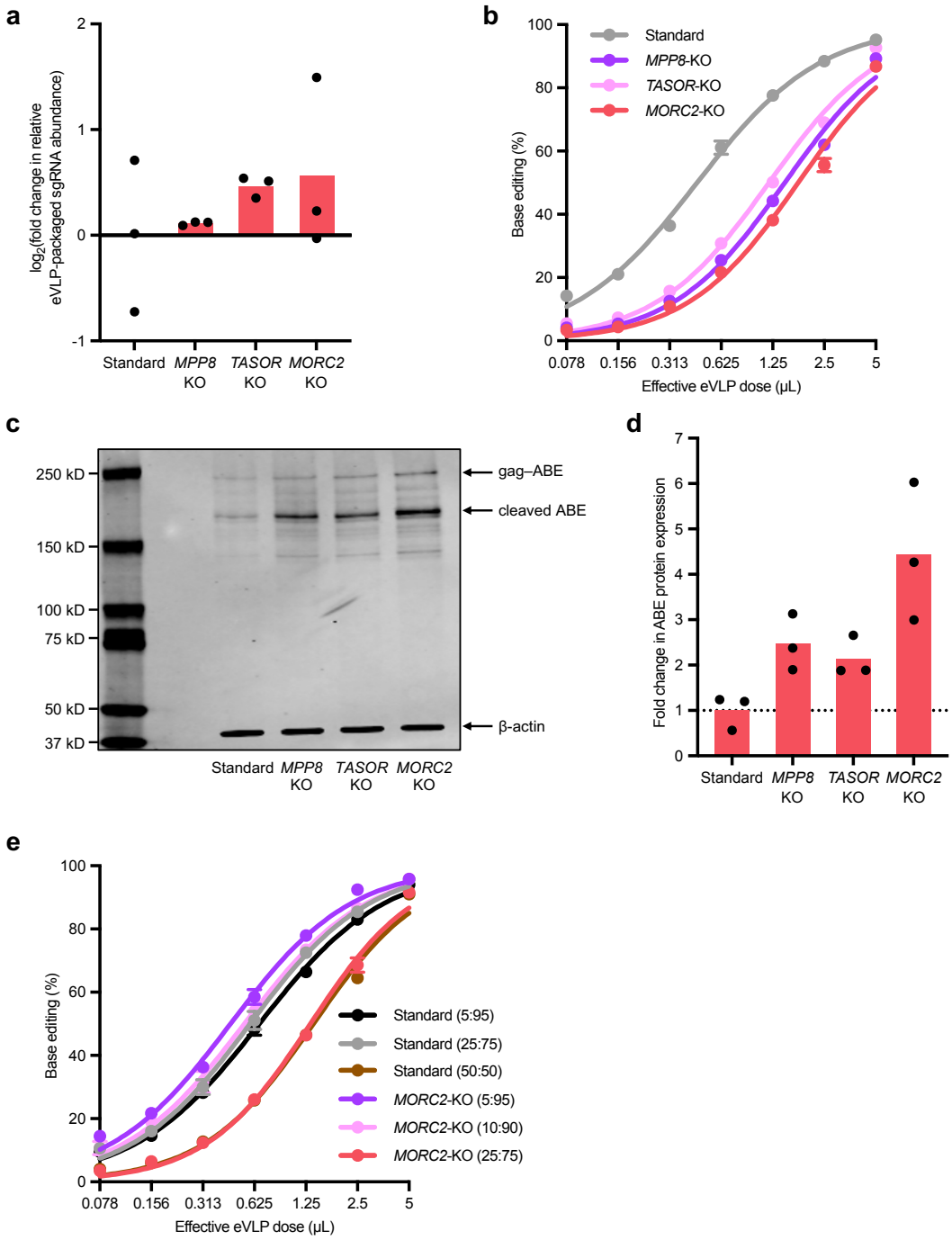

Extended Data Fig. 4 | HUSH-knockout producer cells exhibit increased eVLP protein cargo expression. a, Fold change in eVLP-packaged sgRNA abundance measured by RT-qPCR, normalized relative to sgRNA abundance in eVLPs produced from Gesicle cells. Bars reflect the mean of n=3 replicates, and dots represent individual replicate values. **b**, Comparison of v4 ABE-eVLPs produced from Gesicle or HUSH-knockout cells across a range of eVLP doses. Adenine base editing efficiencies at position A_7 of the *BCL11A* +58 enhancer site in HEK293T cells are shown. **c**, Western

547 blot analysis of protein lysates from producer cells transfected with eVLP production
548 plasmids. The full-length gag–ABE fusion is ~247 kD and the cleaved ABE (following viral
549 protease-mediated cleavage) is ~184 kD. **d**, Fold change in transfected-producer-cell
550 ABE protein abundance measured by Western blot, normalized relative to ABE protein
551 abundance in transfected Gesicle cells. Bars reflect the mean of n=3 replicates, and dots
552 represent individual replicate values. **e**, Comparison of v4 ABE-eVLPs produced from
553 Gesicle or *MORC2*-knockout cells across a range of eVLP doses using different
554 transfected eVLP plasmid stoichiometries. Values in parentheses reflect the gag–
555 ABE:gag–pro–pol plasmid ratio used for eVLP production. Adenine base editing
556 efficiencies at position A_7 of the *BCL11A* +58 enhancer site in HEK293T cells are shown.
557 In **b** and **e**, dots and error bars represent mean ± s.d. of n=3 biological replicates. Data
558 were fit to four-parameter logistic curves using nonlinear regression.

a

	eVLP	ENVLPE⁺	miniEDV	RIDE	VEDIC
Scaffold protein	MMLVgag	HIVgag	HIV "miniGag"	HIVgag	CD63
Cargo loading mechanism	Scaffold–cargo protein fusion	sgRNA aptamer:ABP interaction (PP7:PCP)	Scaffold–cargo protein fusion	sgRNA aptamer:ABP interaction (MS2:MCP)	Scaffold–cargo protein fusion

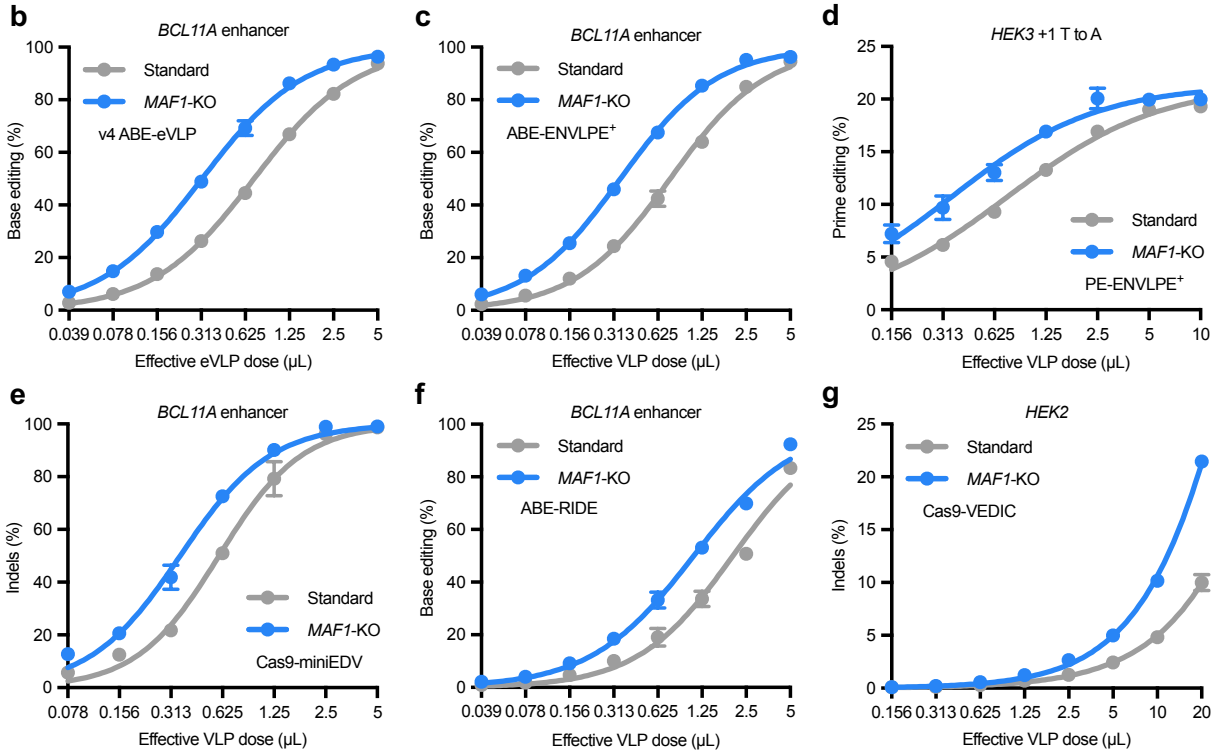

Extended Data Fig. 5 | *MAF1*-knockout producer cells improve delivery potency across various particle types. a, Summary of RNP-packaging particles that were tested. **b**, Comparison of ABE-packaging eVLPs produced from standard or *MAF1*-knockout Gesicle cells across a range of doses. Adenine base editing efficiencies at position A_7 of the *BCL11A* +58 enhancer site in HEK293T cells are shown. **c**, Comparison of ABE-packaging ENVLPE⁺ particles produced from standard or *MAF1*-knockout Gesicle cells across a range of doses. Adenine base editing efficiencies at position A_7 of the *BCL11A* +58 enhancer site in HEK293T cells are shown. **d**, Comparison of PE-packaging ENVLPE⁺ particles produced from standard or *MAF1*-knockout Gesicle cells across a range of doses. +1 T-to-A prime editing efficiencies at the *HEK3* site in HEK293T cells are shown. **e**, Comparison of Cas9-packaging miniEDV particles produced from standard or *MAF1*-knockout Gesicle cells across a range of doses. Indel frequences at the *BCL11A* +58 enhancer site in HEK293T cells are shown. **f**, Comparison of ABE-packaging RIDE particles produced from standard or *MAF1*-knockout Gesicle cells across a range of doses. Adenine base editing efficiencies at position A_7 of the *BCL11A* +58 enhancer site in HEK293T cells are shown. **g**, Comparison of Cas9-packaging VEDIC particles produced from standard or *MAF1*-knockout Gesicle cells across a range of doses. Indel frequencies at the *HEK2* site in HEK293T cells are shown. **b–g**, Dots and error bars

578 represent mean ± s.d. of n=3 biological replicates. Data were fit to four-parameter logistic
579 curves using nonlinear regression.

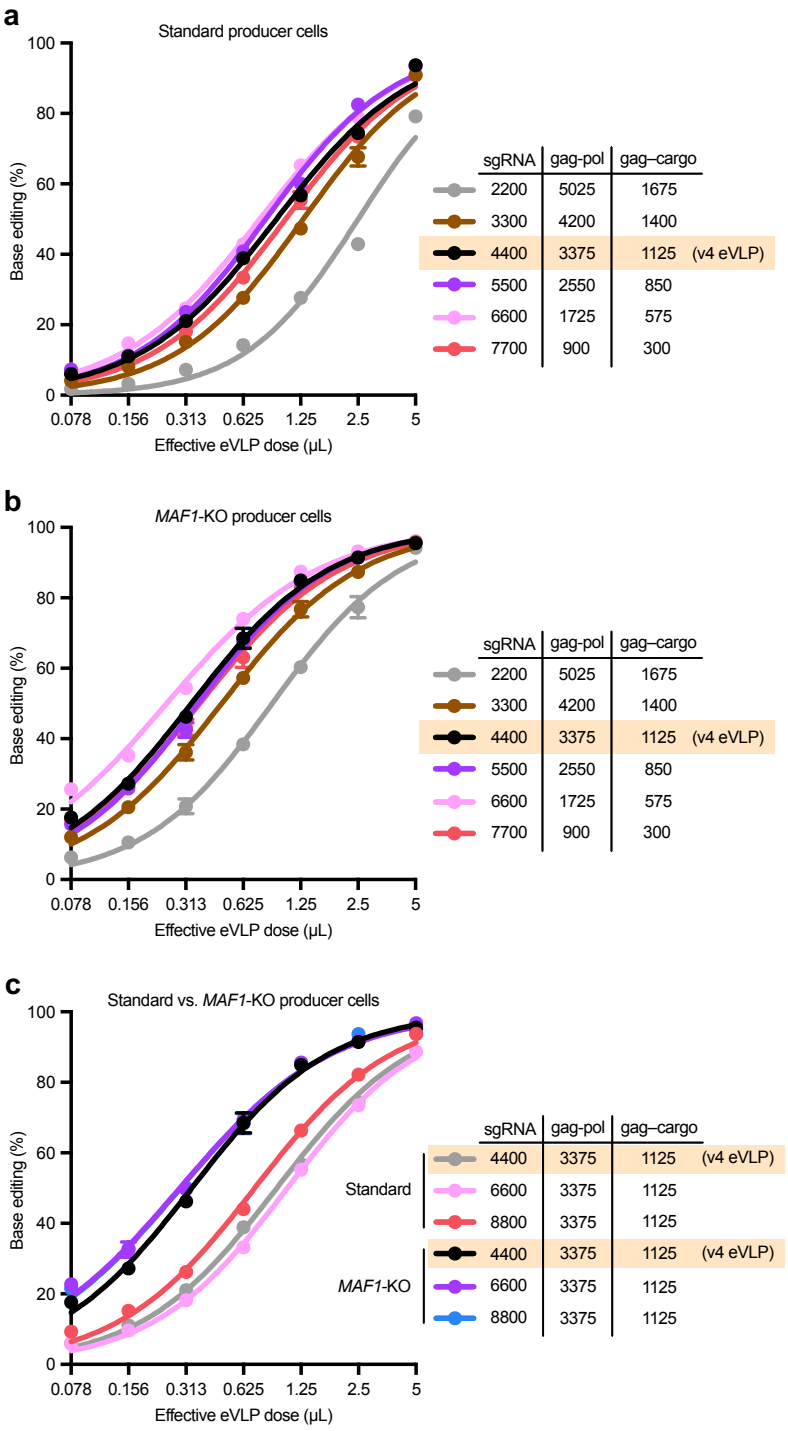

Extended Data Fig. 6 | Increasing sgRNA plasmid amounts does not improve eVLP delivery potency. a–b, Comparison of v4 ABE-eVLPs produced using different sgRNA plasmid amounts (relative to other packaging components) from standard (**a**) or *MAF1*-knockout (**b**) Gesicle cells across a range of doses. **c**, Comparison of v4 ABE-eVLPs produced using different sgRNA plasmid amounts (supplemented in addition to standard packaging components) from standard or *MAF1*-knockout Gesicle cells across a range of doses. **a–c**, Adenine base editing efficiencies at position A_7 of the *BCL11A* +58

587 enhancer site in HEK293T cells are shown. Dots and error bars represent mean ± s.d. of
588 n=3 biological replicates. Data were fit to four-parameter logistic curves using nonlinear
589 regression.

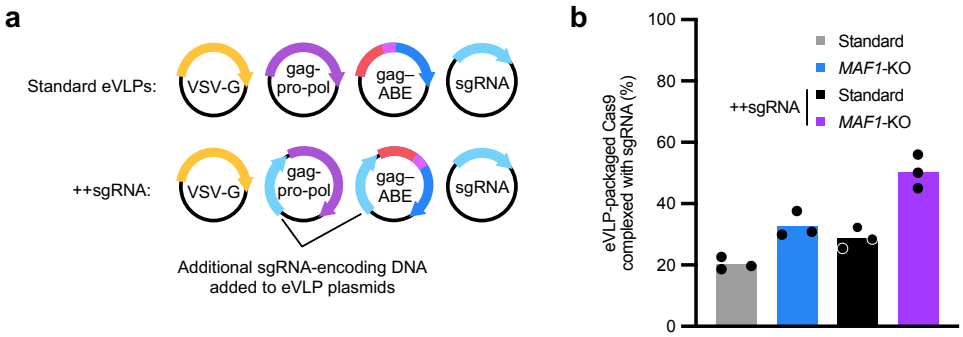

Extended Data Fig. 7 | Adding sgRNA expression cassettes to eVLP packaging plasmids improves eVLP sgRNA packaging. a, Schematic of additional sgRNA expression cassettes (++sgRNA) added to eVLP packaging plasmids (gag–pro–pol and gag–ABE). **b**, Percentage of eVLP-packaged Cas9 molecules that are complexed with sgRNAs. Absolute sgRNA amounts were quantified by RT-qPCR using *in vitro*-transcribed sgRNA standards, and absolute Cas9 protein amounts were quantified by anti-Cas9 ELISA (see Methods). Bars reflect the mean of n=3 replicates, and dots represent individual replicate values.

Methods

Cloning

Plasmids used in this study were cloned via Gibson cloning (NEBuilder® HiFi DNA Assembly; E2621X) or Golden Gate cloning. DNA was amplified via PCR using Phusion HotStart II polymerase (Thermo Fisher Scientific; F537L). Mach1 (Thermo Fisher Scientific; C862003) or NEB® Stable (New England Biolabs; C3040H) chemically competent *E. coli* were used for plasmid propagation. Plasmids were isolated using QIAGEN Plasmid Plus Midi (12945) or Maxi (12963) Kits according to the manufacturer's protocols.

Cell culture

HEK293T cells (ATCC; CRL-3216), Gesicle Producer 293T cells (Takara; 632617), HEK293T/17 cells (ATCC; CRL-11268), and Neuro-2a cells (ATCC; CCL-131) were maintained in DMEM + GlutaMAX (Life Technologies; 10569044) supplemented with 10% (v/v) fetal bovine serum (Gibco; A5670701). Cells were cultured at 37 °C with 5% carbon dioxide and were confirmed to be negative for mycoplasma by testing with MycoAlert (Lonza; LT07-318).

eVLP production and purification

eVLPs were produced as described previously[8,22]. Briefly, eVLPs were produced by transient transfection of Gesicle 293T cells, HEK293T/17 cells, or variants thereof as noted in the main text and figure legends. Producer cells were seeded in T-75 flasks at a density of 5×10^6 cells per flask in 10 mL of media. After 20–24 h, cells were transfected using the jetPRIME transfection reagent (Polyplus; 114-75) according to the manufacturer's protocols. For producing eVLPs, a mixture of plasmids expressing VSV-G (400 ng), MMLV gag–pro–pol (3,375 ng), gag–cargo (1,125 ng), and an sgRNA (4,400 ng) was co-transfected per T-75 flask.

40–48 h post-transfection, producer cell supernatant was harvested and centrifuged for 5 min at 500 g to remove cell debris. The clarified eVLP-containing supernatant was filtered through a 0.45-µm PVDF filter (Millipore; SE1M003M00). The filtered supernatant was concentrated 100-fold using PEG-it Virus Precipitation Solution (System Biosciences; LV825A-1) according to the manufacturer's protocols and resuspended in Opti-MEM serum-free media (Thermo Fisher Scientific; 31985070). For eVLPs prepared for protein or RNA quantification, or those that were injected into mice, the filtered supernatant was concentrated 1500-fold by ultracentrifugation using a cushion of 20% (w/v) sucrose in PBS. Ultracentrifugation was performed at 26,500 rpm (86,242 g) for 2 h (4ºC) using an SW32 Ti rotor in an Optima XE Ultracentrifuge (Beckman Coulter). Following ultracentrifugation, eVLP pellets were resuspended in cold PBS pH 7.4 (Gibco; 10010023) and centrifuged at 1,000 g for 5 min to remove debris. eVLPs were frozen at a rate of -1ºC/min and stored at -80ºC. eVLPs were thawed on ice immediately prior to use.

eVLP transduction and genomic DNA isolation

Cells were transduced with eVLPs as described previously[8,22] with a few modifications. Cells were plated for transduction in 96-well plates at a density of 16,000 cells per well.

After 20–24 h, eVLPs (that were concentrated 100-fold using PEG precipitation described above) were added directly to the culture media in each well. In almost all cases, eVLPs were serially diluted by 2-fold to generate dose titration curves, and a constant volume of 5 µL of eVLP-containing solution was added to each well. For certain experiments, a constant volume of 10 or 20 µL of VLP-containing solution was added to each well, as noted in the appropriate subfigures. 48–72 h post-transduction, cellular genomic DNA was isolated. Media was aspirated from each well, and 60 µL of lysis buffer (10 mM Tris-HCl pH 8.0, 0.05% SDS, 25 µg mL^{-1} Proteinase K (Thermo Fisher Scientific; EO0492)) was added to each well. Lysis was achieved by incubation at 37 ºC for 1–1.5 h followed by heat inactivation at 80ºC for 30 min.

High-throughput sequencing of genomic DNA

Genomic DNA was isolated as described above. Following genomic DNA isolation, 1 µL of the isolated DNA (1–10 ng) was used as input for the first of two PCR reactions. Genomic loci were amplified in PCR1 using Phusion U polymerase (Thermo Fisher Scientific; F562L). PCR1 primers are listed in Supplementary Tables 2 and 7 under the HTS_forward and HTS_reverse columns. PCR1 was performed as follows: 95 ºC for 3 min; 30 cycles of 95 ºC for 15 s, 61 ºC for 20 s, and 72 ºC for 30s; 72ºC for 1 min. PCR1 products were confirmed on a 1% agarose gel. 1 µL of PCR1 was used as an input for PCR2 to install Illumina barcodes. PCR2 was conducted for nine cycles of amplification using Phusion HotStart II polymerase (Thermo Fisher Scientific; F537L). Following PCR2, samples were pooled and gel purified in a 1% agarose gel using a QIAquick Gel Extraction Kit (Qiagen; 28704). Library concentration was quantified using the Qubit™ dsDNA High-Sensitivity Assay Kit (Thermo Fisher Scientific; Q33230). Samples were sequenced on an Illumina MiSeq instrument (paired-end read, read 1: 200–280 cycles, read 2: 0 cycles) using an Illumina MiSeq 300 v2 Kit (Illumina).

High-throughput sequencing data analysis for gene editing experiments

Sequencing reads were demultiplexed using the MiSeq Reporter software (v2.6) (Illumina) and were analyzed using CRISPResso2 (ref. [53]) (v2.3.2) as previously described[8]. Batch analysis mode (one batch for each unique amplicon and sgRNA combination analyzed) was used in all cases. Reads were filtered by minimum average quality score (Q > 30) prior to analysis. For analysis of base editing efficiencies, the following quantification window parameters were used: -w 20 -wc -10. Base editing efficiencies are reported as the percentage of sequencing reads containing a given base conversion at a specific position. For analysis of prime editing efficiencies, the following quantification parameters were used: -w 30 -wc -3 –dicard_indel_reads. Prime editing efficiencies are reported as the number of reads aligned to the edited amplicon sequence divided by the number of reads aligned to all amplicons multiplied by 100. Prism 10 (GraphPad) was used to generate dot plots and bar plots. Amplicon sequences are provided in Supplementary Tables 2 and 7.

Lentiviral vector production

Lentiviral vectors were constructed via Golden Gate cloning into the LentiCRISPRv2-Opti backbone, a gift from the Whitehead Institute Functional Genomics Platform (Addgene #163126). Plasmids were propagated in NEB® Stable (New England Biolabs; C3040H)

692 chemically competent *E. coli*. Prior to lentiviral vector production, HEK293T/17 cells were
693 maintained in antibiotic-free DMEM supplemented with 10% fetal bovine serum (v/v). On
694 day 1, 5×10^6 cells were plated in 10 mL of media in T-75 flasks. The following day, cells
695 were transfected with 6 µg of VSV-G envelope plasmid, 9 µg of psPAX2 (plasmid
696 encoding viral packaging proteins) and 9 µg of transfer vector plasmid diluted in 1,500 µL
697 Opti-MEM with 70 µL of FuGENE HD transfection reagent (Promega; E2312). Two days
698 after transfection, media was centrifuged at 500 *g* for 5 min to remove cell debris followed
699 by filtration using a 0.45-µm PVDF vacuum filter (Millipore; SE1M003M00). The filtered
700 supernatant was concentrated using PEG-it Virus Precipitation Solution (System
701 Biosciences; LV825A-1) according to the manufacturer's protocols and resuspended in
702 Opti-MEM serum-free media (Gibco; 31985070).
703
704 **sgRNA library propagation**
705 For the genome-wide knockout screen, a previously described human genome-wide
706 sgRNA library containing 98,077 unique sgRNAs targeting 19,707 genes across the
707 human genome[30] was obtained as a gift from the Whitehead Institute Functional
708 Genomics Platform. sgRNA sequences are listed in Supplementary Table 3. Vectors
709 contained pU6-sgRNA expression cassettes along with pEFS-Cas9-P2A-PuroR
710 (LentiCRISPRv2-Opti backbone, Addgene #163126). The plasmid library was
711 propagated as follows. First, electrocompetent cells were generated from NEB® Stable
712 (New England Biolabs; C3040H) chemically competent *E. coli* by growing single colonies
713 to mid-log phase in LB media containing 10 µg/mL tetracycline and 50 µg/mL
714 streptomycin, collecting cells by centrifugation at 5,000 g for 1 min at 4 ºC, washing with
715 cold 10% (v/v) glycerol, and repeating for a total of four washes. Freshly prepared
716 electrocompetent cells were transferred to a chilled 0.1 cm electroporation cuvette (Bio-
717 Rad; 1652089) and mixed with the purified, assembled library plasmids. Cells were
718 electroporated using a time-constant protocol with t = 5 ms at 1.5 kV. Electroporated cells
719 were recovered at 37 ºC for 25 min with shaking. Recovered cells were plated onto 500
720 cm^2 plates containing LB media + 1.5% agar supplemented with 100 µg/mL carbenicillin
721 and incubated for 16 h at 37 ºC. After overnight incubation, colonies were scraped into
722 LB media and cells were collected by centrifugation. Plasmids were purified using a
723 Plasmid Plus Maxi Kit (Qiagen; 12963) according to the manufacturer's protocols. sgRNA
724 representation in the propagated plasmid library was confirmed via targeted amplicon
725 sequencing.
726
727 **Genome-wide knockout screen for cargo-loaded eVLP production**
728 Lentiviral libraries were produced as described above and were concentrated ~66-fold by
729 PEG precipitation. Gesicle cells were seeded at a density of 1.5×10^7 cells per T-175 and
730 immediately transduced with 105 µL of concentrated lentivirus. A total of 2.4×10^8 Gesicle
731 cells were seeded for transduction. 24 h after transduction, cells were trypsinized and
732 reseeded at half the original density in media supplemented with 2 µg/mL puromycin.
733 Puromycin selection was continued for 7 days, during which time cell viability was
734 monitored and cells were expanded upon reaching confluency. The initial multiplicity of
735 infection (MOI) was inferred by counting surviving cells and assuming a doubling time of
736 24 h. Using this method, the MOI was calculated to be 0.28, corresponding to

737 approximately 660x coverage of the sgRNA library. A minimum of 1×10^8 cells were carried
738 forward each time the cells were passaged to retain overall coverage.
739 After cells were robustly surviving puromycin selection (~1 week), cells were
740 seeded for eVLP production in T-75 flasks at a density of 5×10^6 cells/flask. At this time,
741 1×10^8 cells were collected by centrifugation, and the cell pellet was frozen at -80ºC and
742 reserved for RNA extraction (see below). 24 h after seeding, cells were transfected using
743 the jetPRIME transfection reagent (Polyplus; 114-75) according to the manufacturer's
744 protocols. A mixture of pUC19 (4,400 ng), VSV-G (400 ng), MMLV gag–pro–pol (3,375
745 ng), and MMLVgag–ABE8e (1,125) plasmids was co-transfected per T-75 flask. 42 h post
746 transfection, eVLPs were harvested and filtered as described above. The filtered
747 supernatant was concentrated by sucrose-cushion ultracentrifugation as described above.
748 Following ultracentrifugation, eVLP pellets were resuspended in cold PBS pH 7.4 (Gibco;
749 10010023). Purified eVLPs were treated with DNase (Qiagen; 79254) followed by RNA
750 extraction using the QIAmp Viral RNA Mini Kit (Qiagen; 52904) according to the
751 manufacturer's protocols. RNA was extracted from the producer-cell pellet using QIAzol
752 Lysis Reagent (Qiagen; 79306) according to the manufacturer's protocols. This entire
753 process of seeding single-knockout Gesicle cells followed by eVLP production and RNA
754 extractions was performed twice on different days for two screen replicates.
755 Following RNA extraction, both producer-cell and eVLP RNA were reverse
756 transcribed using the Maxima Reverse Transcriptase (Thermo Fisher Scientific; EP0742)
757 according to the manufacturer's protocols. Primers and other oligonucleotides used for
758 target-primed sgRNA reverse transcription are listed in Supplementary Table 1. The RT
759 primer was added at a final concentration of 1 µM in the RT reaction. Following incubation
760 at 50ºC for 20 min, the template-switching oligo (TSO) was spiked in to the reaction at a
761 final concentration of 1 µM. The reaction was incubated for a further 20 min at 50ºC, and
762 heat inactivated at 85ºC for 5 min. For producer-cell RNA only, the RT products were
763 further processed by hydrolyzing the RNA in 0.2 M NaOH (final concentration) and
764 heating at 90ºC for 10 min, cleaning up with the MinElute Reaction Cleanup Kit (Qiagen;
765 28104) according to the manufacturer's protocols, and left size selection using SPRIselect
766 (Beckman Coulter; B23317) at a 1.5x bead ratio to remove smaller products and residual
767 primers. Producer-cell cDNAs were subsequently amplified for sequencing with the KAPA
768 HiFi HotStart ReadyMix (Roche Diagnostics; 09420398001) using 2.5 µL of cDNA input
769 per 25 µL reaction and the following conditions: 95 ºC for 3 min; 20 cycles of 98 ºC for 20
770 s, 61 ºC for 20 s, and 72 ºC for 30s; 72ºC for 2 min. eVLP cDNAs were amplified for
771 sequencing with the KAPA HiFi HotStart ReadyMix using 2.5 µL of cDNA input per 25 µL
772 reaction and the following conditions: 95 ºC for 3 min; 14 cycles of 98 ºC for 20 s, 61 ºC
773 for 20 s, and 72 ºC for 30s; 72ºC for 2 min. Illumina barcodes were installed using KAPA
774 HiFi HotStart ReadyMix using 2 µL of PCR1 input per 25 µL reaction and the following
775 conditions: 95 ºC for 3 min; 9 cycles of 98 ºC for 20 s, 61 ºC for 20 s, and 72 ºC for 30s;
776 72ºC for 2 min. Following PCR2, samples were gel purified in a 1% agarose gel using a
777 QIAquick Gel Extraction Kit (Qiagen; 28704). Library concentration was quantified using
778 the Qubit High-Sensitivity Assay Kit (Thermo Fisher Scientific; Q33230). Samples were
779 sequenced on an Illumina NextSeq instrument (paired-end read, read 1: 76 cycles, read
780 2: 0 cycles) using an Illumina NextSeq 75-cycle High-Output v2.5 Kit (Illumina).
781
782 **Genome-wide knockout screen analysis**

783 Code used for processing sequencing reads from the genome-wide knockout screen is
784 provided in Supplementary Note 1. Briefly, sequencing reads were demultiplexed using
785 bcl2fastq (v2.20.0.422). Reads were trimmed using seqkit[54] (v2.6.1) to restrict analysis to
786 the UMI and sgRNA protospacer sequences only. Then, reads were UMI-deduplicated
787 using AmpUMI[55] and trimmed with seqkit to remove the UMI and restrict subsequent
788 analysis to the sgRNA protospacer sequences only. Processed reads were aligned to a
789 reference fasta file containing all sgRNA sequences using bowtie[56] (v1.3.1), and sgRNA
790 counts were generated from alignments as previously described[30]. Raw sgRNA counts
791 are provided in Supplementary Table 4. MAGeCK[57] (v0.5.9.5) was used to quantify gene-
792 level phenotypes from the sgRNA counts. Producer-cell samples were treated as "control"
793 samples and eVLP samples were treated as "treatment" samples for the purpose of
794 MAGeCK analysis. Median-normalized sgRNA read counts and fold changes are
795 provided in Supplementary Table 5, and gene-level phenotypes are provided in
796 Supplementary Table 6. For genes with a positive median $\log_2$ fold change, the positive
797 MAGeCK RRA score, p-value, and FDR were used, and for genes with a negative median
798 $\log_2$ fold change, the negative MAGeCK RRA score, p-value, and FDR were used. Prism
799 10 (GraphPad) was used to generate dot plots.
800
801 **Generation of knockout cell lines**
802 To generate knockout cell lines via Cas9/sgRNA lentiviral transduction, lentiviral vectors
803 were cloned and produced as described above. Cells were seeded in T-75 flasks at a
804 density of 5×10^6 cells/flask and immediately transduced with 50 µL of concentrated
805 lentivirus. 24 h after transduction, cells were trypsinized and reseeded in media
806 supplemented with 2 µg/mL puromycin. Puromycin selection was continued, during which
807 time cell viability was monitored and cells were expanded upon reaching confluency. After
808 cells were robustly surviving puromycin selection (~1 week), cells were harvested and
809 genotyped via targeted-amplicon high-throughput sequencing as described above to
810 confirm gene knockout. Cell lines were regularly genotyped over time to confirm
811 continued gene knockout.
812 To generate knockout cell lines via Cas9-eVLP transduction, v4 Cas9-eVLPs were
813 produced as described above. Cells were seeded in 96-well plates at a density of 16,000
814 cells per well. 24 h after seeding, cells were transduced with 5 µL of purified Cas9-eVLPs
815 per well. 72 h after eVLP transduction, cells were harvested and genotyped via targeted-
816 amplicon high-throughput sequencing as described above to confirm gene knockout.
817 Cells were expanded and regularly genotyped over time to confirm continued gene
818 knockout.
819
820 **eVLP-packaged sgRNA extraction and RT-qPCR**
821 eVLPs for RNA extraction were purified via sucrose-cushion ultracentrifugation as
822 described above. Purified eVLPs were treated with DNase (Qiagen; 79254) followed by
823 RNA extraction using the QIAmp Viral RNA Mini Kit (Qiagen; 52904) according to the
824 manufacturer's protocols. Extracted RNA was reverse transcribed using SuperScript™ III
825 First-Strand Synthesis SuperMix (Thermo Fisher Scientific; 18080400) and an sgRNA-
826 specific DNA primer (see Supplementary Table 1) according to the manufacturer's
827 protocols. qPCR analysis of the resulting cDNA was performed using a QuantStudio™ 3
828 Real-Time PCR System (Thermo Fisher Scientific) with SYBR green dye (Lonza; 50512).

829 The relative eVLP-packaged sgRNA abundance was calculated as $\log_2$[fold change] (ΔC_t)
830 relative to control eVLPs (i.e. those produced from standard or *AAVS1*-knockout cells).
831
832 **Producer-cell RNA extraction and RT-qPCR**
833 Cellular RNA was extracted using the RNeasy Plus Mini Kit (Qiagen; 74136) according
834 to the manufacturer's protocols. Extracted RNA was reverse transcribed using
835 SuperScript™ III First-Strand Synthesis SuperMix (Thermo Fisher Scientific; 18080400)
836 using random hexamer primers according to the manufacturer's protocols. qPCR analysis
837 of the resulting cDNA was performed using a QuantStudio™ 3 Real-Time PCR System
838 (Thermo Fisher Scientific) with SYBR green dye (Lonza; 50512). The relative Cas9
839 mRNA abundance across different producer cells was calculated via the $\Delta\Delta C_t$ method
840 using *ACTB* as the housekeeping gene. qPCR primers are listed in Supplementary Table
841 1.
842
843 **Producer-cell protein extraction and Western blot analyses**
844 For producer-cell protein extraction, 1×10^6 cells were collected by centrifugation at 500 g
845 for 5 min. Cell pellets were washed once with 1 mL of cold PBS and lysed using RIPA
846 buffer (Thermo Fisher Scientific; 89901) supplemented with cOmplete™ protease
847 inhibitor cocktail (Roche Diagnostics; 11836153001) according to the manufacturer's
848 protocols. Cells were lysed at 4ºC for 30 min with gentle agitation. The lysate was clarified
849 by centrifugation at 10,000 g for 20 min at 4ºC, and the clarified supernatant was
850 combined with 4x Laemmli Sample Buffer (Bio-Rad; 1610747) and heated at 95ºC for 10
851 min. Protein extracts were subsequently separated by electrophoresis at 150 V for 45 min
852 on a NuPAGE 3–8% Tris-Acetate gel (Thermo Fisher Scientific; EA0378BOX) in 1x
853 NuPAGE Tris-Acetate SDS running buffer (Thermo Fisher Scientific; LA0041). Transfer
854 to a PVDF membrane was performed using an iBlot 2 Gel Transfer Device (Thermo Fisher
855 Scientific) at 20 V for 7 min. The membrane was blocked for 1 h at room temperature with
856 rocking in blocking buffer: 1% bovine serum albumin (BSA) and 0.1% Tween-20 in TBS
857 (150 mM NaCl and 50 mM Tris-HCl). After blocking, the membrane was incubated
858 overnight at 4ºC with rocking with mouse anti-Cas9 (Cell Signaling Technology; 14697,
859 1:1000 dilution) and rabbit anti-actin (Cell Signaling Technology; 4970, 1:1000 dilution).
860 The membrane was washed three times with 1xTBST (150 mM NaCl, 0.5% Tween-20,
861 and 50 mM Tris-HCl) for 10 min each time at room temperature, then incubated with goat
862 anti-mouse secondary antibody (LI-COR IRDye 680RD; 926-68070, 1:10000 dilution in
863 blocking buffer) and goat anti-rabbit secondary antibody (LI-COR IRDye 800CW; 926-
864 32211, 1:10000 dilution in blocking buffer) for 1 h at room temperature with rocking. The
865 membrane was washed as before and imaged using an Odyssey Imaging System (LI-
866 COR). Protein abundances were quantified by densitometry using ImageJ (v2.14.0).
867 Cas9 abundances were normalized to the actin abundance within each sample, and
868 comparisons across samples were performed using these actin-normalized values.
869 For protein extraction from cells transfected with eVLP production plasmids, cells
870 were first seeded for eVLP production in T-75 flasks as described above. 24 h after
871 seeding, cells were transfected with all eVLP production plasmids except the VSV-G
872 plasmid. 48 h after transfection, cells were trypsinized and collected by centrifugation,
873 and were then processed as described above.
874

875 **eVLP protein content quantification**
876 eVLP protein content quantification was performed as described previously[8]. Briefly,
877 ultracentrifuge-purified eVLPs were lysed in dye-free Laemmli sample buffer (50 mM Tris-
878 HCl pH 7.0, 2% sodium dodecyl sulfate (SDS), 10% (v/v) glycerol, 2 mM dithiothreitol
879 (DTT)) by heating at 95ºC for 15 min. The concentration of ABE protein in purified eVLPs
880 was quantified using the FastScan™ Cas9 (*S. pyogenes*) ELISA kit (Cell Signaling
881 Technology; 29666C) according to the manufacturer's protocols. Recombinant Cas9 (*S.*
882 *pyogenes*) nuclease protein (New England Biolabs; M0386) was used to generate the
883 standard curve for quantification. The concentration of MLV p30 protein in purified eVLPs
884 was quantified using the MuLV Core Antigen ELISA kit (Cell Biolabs; VPK-156) according
885 to the manufacturer's protocols. To calculate eVLP titer in particles/μL, the p30
886 concentration in ng/mL determined by ELISA was multiplied by a factor 2030.57, which
887 accounts for molarity conversions, assumes that 20% of p30 molecules in solution are
888 associated with particles, and assumes a copy number of 1800 molecules of p30 per
889 eVLP, as previously described[8]. The number of ABE protein molecules per eVLP was
890 calculated by determining the ratio of Cas9 molecules to p30 molecules and assuming a
891 copy number of 1800 molecules of p30 per eVLP, as previously described[8].
892
893 **Animal experiments**
894 All mouse experiments were compliant with relevant ethical regulations and were
895 approved by the MIT Committee on Animal Care (D16-00078; 2402000629). Wild-type 8-
896 week-old adult male C57BL/6J mice (000664) were purchased from the Jackson
897 Laboratory. All mice were housed in a room maintained on a 12 h light and dark cycle
898 with *ad libitum* access to standard rodent diet and water. Animals were randomly
899 assigned to various experimental groups.
900 Retro-orbital injections were performed as described previously[8] with a few
901 modifications. eVLPs for retro-orbital injections were purified via sucrose-cushion
902 ultracentrifugation as described above. Immediately prior to injection, eVLPs were
903 partially clarified by centrifugation at 1000 g for 5 min to remove debris. The eVLP-
904 containing supernatant was diluted with 0.9% NaCl (Hospira; 00409-4888-10), and a total
905 of 100 μL solution was injected per mouse: 85 μL saline + 15 μL of 1500-fold concentrated
906 purified eVLPs, containing 3×10^{11} eVLPs as was quantified by ELISA using the procedure
907 described above). Genomic DNA was purified from bulk liver tissue using the Agencourt
908 DNAdvance kit (Beckman Coulter; A48705) according to the manufacturer's protocols.
909 Purified genomic DNA was amplified for high-throughput sequencing as described above,
910 with 25 cycles of amplification during PCR1.
911
912 **Production of other VLP constructs**
913 ENVLPE$^+$ particles[10], miniEDVs[44], RIDE VLPs[16], and VEDIC[45] particles were produced
914 analogously to eVLPs. Producer cells were seeded in T-75 flasks at a density of 5×10^6
915 cells per flask. After 20–24 h, cells were transfected using the jetPRIME transfection
916 reagent (Polyplus; 114-75) according to the manufacturer's protocols.
917 For producing ABE-ENVLPE$^+$ particles, a mixture of plasmids expressing VSV-G
918 (1,550 ng), psPAX2-D64V (1,149 ng; Addgene #63586, a gift from David Rawlings &
919 Andrew Scharenberg), pCMV_ENVLPE+ (665 ng; Addgene #232427, a gift from Gil
920 Westmeyer), pCMV_ABE8e_superNLS (1,023 ng; Addgene #232429, a gift from Gil

921 Westmeyer), and a *BCL11A*-targeting PP7-containing sgRNA (4,913 ng; cloned from
922 Addgene #232432, a gift from Gil Westmeyer) was co-transfected per T-75 flask.
923 For producing PE-ENVLPE$^+$ particles, a mixture of plasmids expressing VSV-G
924 (1,550 ng), psPAX2-D64V (1,149 ng; Addgene #63586, a gift from David Rawlings &
925 Andrew Scharenberg), pCMV_ENVLPE+ (665 ng; Addgene #232427, a gift from Gil
926 Westmeyer), pCMV_iPE-C_P2A_Csy4 (1,023 ng; Addgene #232428, a gift from Gil
927 Westmeyer), and pU6_HEK3+1T>A_(PP7-C4-Q1) (4,913 ng; Addgene #232437, a gift
928 from Gil Westmeyer) was co-transfected per T-75 flask.
929 For producing miniEDVs, a mixture of plasmids expressing VSV-G (930 ng), a
930 *BCL11A*-targeting sgRNA and miniGag (2,790 ng; cloned from Addgene #228957, a gift
931 from Jennifer Doudna), and a *BCL11A*-targeting sgRNA and miniGag–Cas9 (5,580 ng;
932 cloned from Addgene #228958, a gift from Jennifer Doudna) was co-transfected per T-75
933 flask.
934 For producing RIDE VLPs, a mixture of plasmids expressing VSV-G (760 ng),
935 pRSV-Rev (610 ng; Addgene #12253, a gift from Didier Trono), pMS2M-PH-gagpol-D64V
936 (1,320 ng; Addgene #166031, a gift from Yujia Cai), pMDLg/pRRE (1,320 ng; Addgene
937 #12251, a gift from Didier Trono), ABE8e (2,640 ng; Addgene #138489, a gift from David
938 Liu), and a *BCL11A*-targeting MS2-containing sgRNA (2,640; Addgene #229772, a gift
939 from Yujia Cai) was co-transfected per T-75 flask.
940 For producing VEDIC particles, a mixture of plasmids expressing VSV-G (400 ng),
941 a CD63–intein–Cas9 fusion (3,500 ng), and *HEK2*-targeting sgRNA (5,400 ng) was co-
942 transfected per T-75 flask.
943 For all VLPs, 40–48 h post-transfection, producer cell supernatant was harvested
944 and centrifuged for 5 min at 500 g to remove cell debris. The clarified VLP-containing
945 supernatant was filtered through a 0.45-μm PVDF filter (Millipore; SE1M003M00). The
946 filtered supernatant was concentrated 100-fold using PEG-it Virus Precipitation Solution
947 (System Biosciences; LV825A-1) according to the manufacturer's protocols and
948 resuspended in Opti-MEM serum-free media (Thermo Fisher Scientific; 31985070). For
949 all VLPs, transduction of HEK293T cells was performed as described above for eVLPs.
950
951 **Quantification of eVLP-packaged Cas9 molecules complexed with sgRNAs**
952 For each construct, the number of Cas9 molecules per unit volume of eVLPs was
953 calculated via anti-Cas9 ELISA as described above. For sgRNA quantification, purified
954 eVLPs were treated with DNase (Qiagen; 79254). Then, 100 ng of 151-bp spike-in RNA
955 (see below) was added to each sample, followed by RNA extraction using the QIAmp
956 Viral RNA Mini Kit (Qiagen; 52904) according to the manufacturer's protocols. Extracted
957 RNA was reverse transcribed using SuperScript™ III First-Strand Synthesis SuperMix
958 (Thermo Fisher Scientific; 18080400) and both an sgRNA-specific DNA primer and a
959 spike-in RNA-specific DNA primer (see Supplementary Table 1) according to the
960 manufacturer's protocols. qPCR analysis of the resulting cDNA was performed with both
961 sgRNA-specific and spike-in RNA-specific primers (see Supplementary Table 1) using a
962 QuantStudio™ 3 Real-Time PCR System (Thermo Fisher Scientific) with SYBR green
963 dye (Lonza; 50512).
964 To determine the absolute amount of sgRNA and spike-in cDNA in each sample,
965 a standard curve for each cDNA species was generated. First, RNA standards for both
966 species were generated via *in vitro* transcription using the HiScribe® T7 Quick High Yield

RNA Synthesis Kit (New England Biolabs; E2050S). Transcribed RNA yield was quantified using the Qubit™ RNA High-Sensitivity Assay Kit (Thermo Fisher Scientific; Q32852). Then, serial dilutions of each RNA standard were made in water, and the resulting diluted RNAs were subjected to reverse transcription using either sgRNA-specific or spike-in RNA-specific DNA primers as described above. The resulting cDNAs were used as input into qPCR reactions to generate a standard curve for each cDNA species.

Standard curves were analyzed via linear regression using Prism 10 (GraphPad), and these curves were used to calculate the number of sgRNA and spike-in RNA molecules present in each eVLP-derived sample after RNA extraction. To determine the number of sgRNA molecules present in each eVLP sample before RNA extraction, RNA loss during the extraction process was accounted for by calculating the percent recovery of spike-in RNA for each sample (using the knowledge that exactly 100 ng of spike-in RNA was added to each sample before RNA extraction, as described above). Using this RNA recovery factor, the number of sgRNA molecules present in each eVLP sample before RNA extraction was calculated (with the assumption that, for each sample, the percent recovery of spike-in RNA and sgRNA are equal since both species are of similar size). Finally, the percentage of eVLP-packaged Cas9 molecules complexed with sgRNAs was calculated for each sample by dividing the number of sgRNA molecules per unit volume of eVLPs by the number of Cas9 molecules per unit volume of eVLPs. This calculation assumes that all sgRNA molecules detected in eVLPs are complexed with Cas9 molecules, since sgRNA packaging into eVLPs in the absence of Cas9 is negligible[22].

Statistical analysis

Data are presented as mean and standard deviation (s.d.). No statistical methods were used to predetermine sample size. Statistical analysis was performed using Prism 10 (GraphPad). Sample sizes are described in the figure legends.

Data availability

The high-throughput sequencing data generated during this study is being deposited at the NCBI Sequence Read Archive database under PRJNA1288558. Raw data from the genome-wide knockout screen is provided in Supplementary Tables 3–6. Key plasmids from this work will be deposited to Addgene for distribution. Other plasmids and cell lines are available from the corresponding author on request.

Code availability

The code used for analyzing base editing efficiencies are available at https://github.com/pinellolab/CRISPResso2. The code used for analyzing CRISPR screen results are available in Supplementary Note 1 and at https://sourceforge.net/p/mageck/wiki/Home/.

Acknowledgements

This work was supported by the Whitehead Institute and Whitehead Fellows Program (A.R.); NIH Director's Early Independence Award DP5OD037342 (A.R.); Merkin Institute for Transformative Technologies in Healthcare (A.R.); McGuire Family Foundation (A.R.);

James M. and Cathleen D. Stone Foundation (A.R.); Owens Family Foundation (A.R.); and Valhalla Foundation (A.R.). H.J. acknowledges support from the National Research Foundation of Korea. A.S. was supported by the Whitehead Scholars Program at Williams College. We thank H. Keys and the Functional Genomics Platform at Whitehead Institute for providing the genome-wide sgRNA library used in our study; A. Nelson, D. Liu, and the Whitehead Genome Technology Core for access to Illumina sequencing instrumentation; and the Jain, Reddien, Weissman, and Young Labs for generous access to equipment.

Author contributions

A.R. conceived the project. D.L., H.J., A.G., A.S., and A.R. designed the research, performed experiments, and analyzed data. H.J. performed mouse experiments. A.R. wrote the manuscript, and all authors edited the manuscript.

Competing interests

The authors declare competing financial interests: D.L. and A.R. have filed a patent application on this work through the Whitehead Institute. The remaining authors declare no competing interests.

1031 **References**
1032

1033 1. Raguram, A., Banskota, S. & Liu, D.R. Therapeutic in vivo delivery of gene editing
1034 agents. *Cell* **185**, 2806-2827 (2022).

1035 2. van Haasteren, J., Li, J., Scheideler, O.J., Murthy, N. & Schaffer, D.V. The delivery
1036 challenge: fulfilling the promise of therapeutic genome editing. *Nat Biotechnol* **38**,
1037 845-855 (2020).

1038 3. Wang, D., Zhang, F. & Gao, G. CRISPR-Based Therapeutic Genome Editing:
1039 Strategies and In Vivo Delivery by AAV Vectors. *Cell* **181**, 136-150 (2020).

1040 4. Wei, T. et al. Delivery of Tissue-Targeted Scalpels: Opportunities and Challenges
1041 for In Vivo CRISPR/Cas-Based Genome Editing. *ACS Nano* **14**, 9243-9262 (2020).

1042 5. Wang, J.Y. & Doudna, J.A. CRISPR technology: A decade of genome editing is
1043 only the beginning. *Science* **379**, eadd8643 (2023).

1044 6. Tsuchida, C.A., Wasko, K.M., Hamilton, J.R. & Doudna, J.A. Targeted nonviral
1045 delivery of genome editors in vivo. *Proc Natl Acad Sci U S A* **121**, e2307796121
1046 (2024).

1047 7. An, M. et al. Engineered virus-like particles for transient delivery of prime editor
1048 ribonucleoprotein complexes in vivo. *Nat Biotechnol* **42**, 1526-1537 (2024).

1049 8. Banskota, S. et al. Engineered virus-like particles for efficient in vivo delivery of
1050 therapeutic proteins. *Cell* **185**, 250-265 e216 (2022).

1051 9. Choi, J.G. et al. Lentivirus pre-packed with Cas9 protein for safer gene editing.
1052 *Gene Ther* **23**, 627-633 (2016).

1053 10. Geilenkeuser, J. et al. Engineered nucleocytosolic vehicles for loading of
1054 programmable editors. *Cell* **188**, 2637-2655 e2631 (2025).

1055 11. Haldrup, J. et al. Engineered lentivirus-derived nanoparticles (LVNPs) for delivery of
1056 CRISPR/Cas ribonucleoprotein complexes supporting base editing, prime editing
1057 and in vivo gene modification. *Nucleic Acids Res* **51**, 10059-10074 (2023).

1058 12. Halegua, T. et al. Delivery of Prime editing in human stem cells using pseudoviral
1059 NanoScribes particles. *Nat Commun* **16**, 397 (2025).

1060 13. Hamilton, J.R. et al. In vivo human T cell engineering with enveloped delivery
1061 vehicles. *Nat Biotechnol* **42**, 1684-1692 (2024).

1062 14. Hamilton, J.R. et al. Targeted delivery of CRISPR-Cas9 and transgenes enables
1063 complex immune cell engineering. *Cell Rep* **35**, 109207 (2021).

1064 15. Indikova, I. & Indik, S. Highly efficient 'hit-and-run' genome editing with
1065 unconcentrated lentivectors carrying Vpr.Prot.Cas9 protein produced from RRE-
1066 containing transcripts. *Nucleic Acids Res* **48**, 8178-8187 (2020).

1067 16. Ling, S. et al. Customizable virus-like particles deliver CRISPR-Cas9
1068 ribonucleoprotein for effective ocular neovascular and Huntington's disease gene
1069 therapy. *Nat Nanotechnol* **20**, 543-553 (2025).

1070 17. Lu, Z. et al. Lentiviral Capsid-Mediated Streptococcus pyogenes Cas9
1071 Ribonucleoprotein Delivery for Efficient and Safe Multiplex Genome Editing.
1072 *CRISPR J* **4**, 914-928 (2021).

1073 18. Lyu, P., Javidi-Parsijani, P., Atala, A. & Lu, B. Delivering Cas9/sgRNA
1074 ribonucleoprotein (RNP) by lentiviral capsid-based bionanoparticles for efficient 'hit-
1075 and-run' genome editing. *Nucleic Acids Res* **47**, e99 (2019).

1076 19. Lyu, P. et al. Adenine Base Editor Ribonucleoproteins Delivered by Lentivirus-Like
1077 Particles Show High On-Target Base Editing and Undetectable RNA Off-Target
1078 Activities. *CRISPR J* **4**, 69-81 (2021).

1079 20. Lyu, P., Wang, L. & Lu, B. Virus-Like Particle Mediated CRISPR/Cas9 Delivery for
1080 Efficient and Safe Genome Editing. *Life (Basel)* **10** (2020).

1081 21. Mangeot, P.E. et al. Genome editing in primary cells and in vivo using viral-derived
1082 Nanoblades loaded with Cas9-sgRNA ribonucleoproteins. *Nat Commun* **10**, 45
1083 (2019).

1084 22. Raguram, A., An, M., Chen, P.Z. & Liu, D.R. Directed evolution of engineered virus-
1085 like particles with improved production and transduction efficiencies. *Nat Biotechnol*
1086 **43**, 1635-1647 (2025).

1087 23. Xu, D. et al. Programmable epigenome editing by transient delivery of CRISPR
1088 epigenome editor ribonucleoproteins. *Nat Commun* **16**, 7948 (2025).

1089 24. Barnes, C.R. et al. Genome-wide activation screens to increase adeno-associated
1090 virus production. *Mol Ther Nucleic Acids* **26**, 94-103 (2021).

1091 25. Iaffaldano, B.J., Marino, M.P. & Reiser, J. CRISPR library screening to develop
1092 HEK293-derived cell lines with improved lentiviral vector titers. *Front Genome Ed* **5**,
1093 1218328 (2023).

1094 26. O'Driscoll, E.E., Arora, S., Lang, J.F., Davidson, B.L. & Shalem, O. CRISPR screen
1095 reveals modifiers of rAAV production including known rAAV infection genes playing
1096 an unexpected role in vector production. *Mol Ther Methods Clin Dev* **33**, 101408
1097 (2025).

1098 27. Tridgett, M. et al. Lentiviral vector packaging and producer cell lines yield titers
1099 equivalent to the industry-standard four-plasmid process. *Mol Ther Methods Clin*
1100 *Dev* **32**, 101315 (2024).

1101 28. Han, J., Tam, K., Tam, C., Hollis, R.P. & Kohn, D.B. Improved lentiviral vector titers
1102 from a multi-gene knockout packaging line. *Mol Ther Oncolytics* **23**, 582-592
1103 (2021).

1104 29. Xinyue, Z. et al. Engineering of HEK293T Cell Factory for Lentiviral Production by
1105 High-Throughput Selected Genes. *CRISPR J* **7**, 272-282 (2024).

1106 30. Lam, B. et al. Multi-species genome-wide CRISPR screens identify conserved
1107 suppressors of cold-induced cell death. *eLife*, 10.7554/eLife.102310.102311 (2024).

1108 31. Replogle, J.M. et al. Combinatorial single-cell CRISPR screens by direct guide RNA
1109 capture and targeted sequencing. *Nat Biotechnol* **38**, 954-961 (2020).

1110 32. Seczynska, M., Bloor, S., Cuesta, S.M. & Lehner, P.J. Genome surveillance by
1111 HUSH-mediated silencing of intronless mobile elements. *Nature* **601**, 440-445
1112 (2022).

1113 33. Seczynska, M. & Lehner, P.J. The sound of silence: mechanisms and implications
1114 of HUSH complex function. *Trends Genet* **39**, 251-267 (2023).

1115 34. DeKelver, R.C. et al. Functional genomics, proteomics, and regulatory DNA
1116 analysis in isogenic settings using zinc finger nuclease-driven transgenesis into a
1117 safe harbor locus in the human genome. *Genome Res* **20**, 1133-1142 (2010).

1118 35. Liao, J. et al. Therapeutic adenine base editing of human hematopoietic stem cells.
1119 *Nat Commun* **14**, 207 (2023).

1120 36. Johnson, S.S., Zhang, C., Fromm, J., Willis, I.M. & Johnson, D.L. Mammalian Maf1
1121 is a negative regulator of transcription by all three nuclear RNA polymerases. *Mol*
1122 *Cell* **26**, 367-379 (2007).

1123 37. Vannini, A. et al. Molecular basis of RNA polymerase III transcription repression by
1124 Maf1. *Cell* **143**, 59-70 (2010).

1125 38. Vorlander, M.K. et al. Structural basis for RNA polymerase III transcription
1126 repression by Maf1. *Nat Struct Mol Biol* **27**, 229-232 (2020).

1127 39. Musunuru, K. et al. In vivo CRISPR base editing of PCSK9 durably lowers
1128 cholesterol in primates. *Nature* **593**, 429-434 (2021).

1129 40. Levy, J.M. et al. Cytosine and adenine base editing of the brain, liver, retina, heart
1130 and skeletal muscle of mice via adeno-associated viruses. *Nat Biomed Eng* **4**, 97-
1131 110 (2020).

1132 41. Bauler, M. et al. Production of Lentiviral Vectors Using Suspension Cells Grown in
1133 Serum-free Media. *Mol Ther Methods Clin Dev* **17**, 58-68 (2020).

1134 42. Richter, M.F. et al. Phage-assisted evolution of an adenine base editor with
1135 improved Cas domain compatibility and activity. *Nat Biotechnol* **38**, 883-891 (2020).

1136 43. Neugebauer, M.E. et al. Evolution of an adenine base editor into a small, efficient
1137 cytosine base editor with low off-target activity. *Nat Biotechnol* **41**, 673-685 (2023).

1138 44. Ngo, W. et al. Mechanism-guided engineering of a minimal biological particle for
1139 genome editing. *Proc Natl Acad Sci U S A* **122**, e2413519121 (2025).

1140 45. Liang, X. et al. Engineering of extracellular vesicles for efficient intracellular delivery
1141 of multimodal therapeutics including genome editors. *Nat Commun* **16**, 4028
1142 (2025).

1143 46. Chen, Y.H. et al. Rapid Lentiviral Vector Producer Cell Line Generation Using a
1144 Single DNA Construct. *Mol Ther Methods Clin Dev* **19**, 47-57 (2020).

1145 47. Lee, Z., Lu, M., Irfanullah, E., Soukup, M. & Hu, W.S. Construction of an rAAV
1146 Producer Cell Line through Synthetic Biology. *ACS Synth Biol* **11**, 3285-3295
1147 (2022).

1148 48. Powers, A.D., Drury, J.E., Hoehamer, C.F., Lockey, T.D. & Meagher, M.M.
1149 Lentiviral Vector Production from a Stable Packaging Cell Line Using a Packed Bed
1150 Bioreactor. *Mol Ther Methods Clin Dev* **19**, 1-13 (2020).

1151 49. Montagna, C. et al. VSV-G-Enveloped Vesicles for Traceless Delivery of CRISPR-
1152 Cas9. *Mol Ther Nucleic Acids* **12**, 453-462 (2018).

1153 50. Kunitake, K. et al. Barcoding of small extracellular vesicles with CRISPR-gRNA
1154 enables comprehensive, subpopulation-specific analysis of their biogenesis and
1155 release regulators. *Nat Commun* **15**, 9777 (2024).

1156 51. Lu, A. et al. Genome-wide interrogation of extracellular vesicle biology using
1157 barcoded miRNAs. *Elife* **7** (2018).

1158 52. Strebinger, D. et al. Cell type-specific delivery by modular envelope design. *Nat*
1159 *Commun* **14**, 5141 (2023).

1160 53. Clement, K. et al. CRISPResso2 provides accurate and rapid genome editing
1161 sequence analysis. *Nat Biotechnol* **37**, 224-226 (2019).

1162 54. Shen, W., Le, S., Li, Y. & Hu, F. SeqKit: A Cross-Platform and Ultrafast Toolkit for
1163 FASTA/Q File Manipulation. *PLoS One* **11**, e0163962 (2016).

1164 55. Clement, K., Farouni, R., Bauer, D.E. & Pinello, L. AmpUMI: design and analysis of
1165 unique molecular identifiers for deep amplicon sequencing. *Bioinformatics* **34**, i202-
1166 i210 (2018).

1167 56. Langmead, B., Trapnell, C., Pop, M. & Salzberg, S.L. Ultrafast and memory-efficient
1168 alignment of short DNA sequences to the human genome. *Genome Biol* **10**, R25
1169 (2009).

1170 57. Li, W. et al. MAGeCK enables robust identification of essential genes from genome-
1171 scale CRISPR/Cas9 knockout screens. *Genome Biol* **15**, 554 (2014).

1172